Article

Cell Metabolism

CD38 Dictates Age-Related NAD Decline and Mitochondrial Dysfunction through an SIRT3-Dependent Mechanism

Graphical Abstract

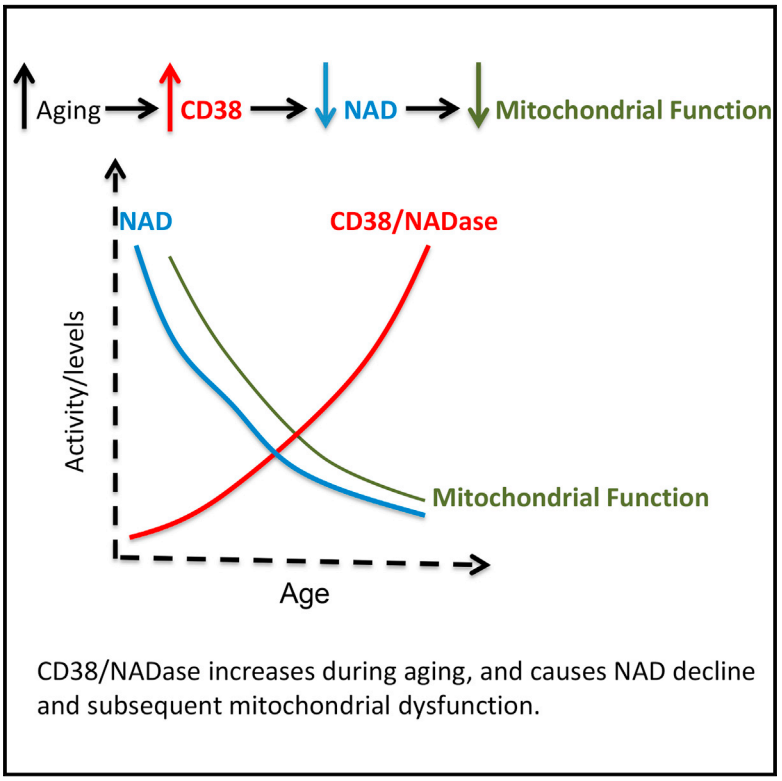

CD38/NADase increases during aging, and causes NAD decline and subsequent mitochondrial dysfunction.

Highlights

- CD38 levels increase in tissues with age and correlate with NAD decline
- NAD and mitochondrial function are preserved in old CD38 knockout mice
- CD38 metabolizes NMN in vivo and modulates the response to NAD-replacement therapy

Authors

Juliana Camacho-Pereira, Mariana G. Tarragó, Claudia C.S. Chini, ..., Joel M. Reid, Antonio Galina, Eduardo N. Chini

Correspondence

chini.eduardo@mayo.edu

In Brief

Why do NAD levels decrease with age? Camacho et al. now reveal that increased expression of the NADase CD38 is responsible for NAD decline and mitochondrial dysfunction in older mice in an SIRT3-dependent manner. CD38 also metabolizes the NAD precursor NMN and modulates the response to NAD-replacement therapy in vivo.

Camacho-Pereira et al., 2016, Cell Metabolism *23*, 1127–1139
June 14, 2016
http://dx.doi.org/10.1016/j.cmet.2016.05.006

CellPress

Cell Metabolism
Article

CD38 Dictates Age-Related NAD Decline and Mitochondrial Dysfunction through an SIRT3-Dependent Mechanism

Juliana Camacho-Pereira,[1,2] Mariana G. Tarragó,[1] Claudia C.S. Chini,[1] Veronica Nin,[1] Carlos Escande,[1] Gina M. Warner,[1] Amrutesh S. Puranik,[1] Renee A. Schoon,[3] Joel M. Reid,[3] Antonio Galina,[2] and Eduardo N. Chini[1,*]
[1]Signal Transduction Laboratory, Kogod Aging Center, Department of Anesthesiology, Mayo Clinic College of Medicine, Rochester, MN 55905, USA
[2]Instituto de Bioquímica Médica, Centro de Ciências da Saúde, Universidade Federal do Rio de Janeiro, Cidade Universitária, Ilha do Fundão, Rio de Janeiro, RJ 21941-590, Brazil
[3]Oncology Research, Mayo Clinic College of Medicine, Rochester, MN 55905, USA
*Correspondence: chini.eduardo@mayo.edu
http://dx.doi.org/10.1016/j.cmet.2016.05.006

SUMMARY

Nicotinamide adenine dinucleotide (NAD) levels decrease during aging and are involved in age-related metabolic decline. To date, the mechanism responsible for the age-related reduction in NAD has not been elucidated. Here we demonstrate that expression and activity of the NADase CD38 increase with aging and that CD38 is required for the age-related NAD decline and mitochondrial dysfunction via a pathway mediated at least in part by regulation of SIRT3 activity. We also identified CD38 as the main enzyme involved in the degradation of the NAD precursor nicotinamide mononucleotide (NMN) in vivo, indicating that CD38 has a key role in the modulation of NAD-replacement therapy for aging and metabolic diseases.

INTRODUCTION

NAD (nicotinamide adenine dinucleotide) is a cofactor of key enzymes in glycolysis, the tricarboxylic acid cycle, and oxidative phosphorylation (Oxphos), participating in multiple redox reactions in cells. It has been shown that the cellular NAD pool is determined by a balance between the activity of NAD-synthesizing and NAD-consuming enzymes (Aksoy et al., 2006; Bai et al., 2011; Barbosa et al., 2007; Nahimana et al., 2009; Yang et al., 2007; Yoshino et al., 2011). Recently, it has been described that NAD levels decline during chronological aging and in progeroid states, leading to mitochondrial dysfunction and metabolic abnormalities (Zhu et al., 2015; Gomes et al., 2013; Braidy et al., 2011; Scheibye-Knudsen et al., 2014; Massudi et al., 2012). Thus, determining the mechanisms that lead to this age-related NAD decline is of great importance for the development of therapies for age-related diseases.

Age-related NAD decline may be caused by an increase in NAD-consuming enzymes (NADases), a decrease in NAD-synthesizing enzymes, or a combination of both. However, to date, the precise contribution of specific metabolic pathways that regulate NAD levels in the age-related NAD decline has not been determined. In the case of NAD consumption, it has been shown that enzymes such as poly (ADP-ribose) polymerases (PARPs), NAD-dependent deacetylases (SIRTUINS), and NADases such as CD38 can degrade this molecule during their catalytic processes (Bai et al., 2011; Bai and Cantó, 2012; Aksoy et al., 2006; Imai and Guarente, 2014). In particular, we have shown that the enzyme CD38 is one of the main NAD-degrading enzymes in mammalian tissues (Aksoy et al., 2006; Barbosa et al., 2007). CD38 was originally identified as a cell-surface enzyme that plays a key role in several physiological processes such as immune response, inflammation, cancer, and metabolic disease (Barbosa et al., 2007; Frasca et al., 2006; Guedes et al., 2008; Malavasi et al., 2008). We have previously shown that CD38 knockout (CD38KO) mice have higher NAD levels and are protected against obesity and metabolic syndrome (Barbosa et al., 2007). In addition, treatment of obese mice with CD38 inhibitors increases intracellular NAD levels and improves several aspects of glucose and lipid homeostasis (Escande et al., 2013). However, the role of CD38 in age-related NAD decline and mitochondrial dysfunction has never been investigated.

Here we show for the first time that CD38 plays an active role in the age-related NAD decline in mammals. NAD levels, mitochondrial respiratory rates, and metabolic functions are preserved during the aging process in CD38KO mice. We further identified that CD38 is the main enzyme metabolizing the NAD precursor NMN in vivo, and demonstrated that ablation of CD38 improves the response to NAD-replacement therapy during aging. We believe that these findings may lead to new strategies for the treatment of diseases related to an imbalance in NAD metabolism and energy homeostasis.

RESULTS

Protein Levels and mRNA Expression of the NADase CD38 Increase with Chronological Aging

Previous studies have suggested that tissue NAD^+ levels decline with aging (Zhu et al., 2015; Gomes et al., 2013; Braidy et al., 2011; Massudi et al., 2012). To confirm the data on NAD decline in aging, we measured NAD^+ and NADH levels in murine tissues by two different methods, the cycling assay and an

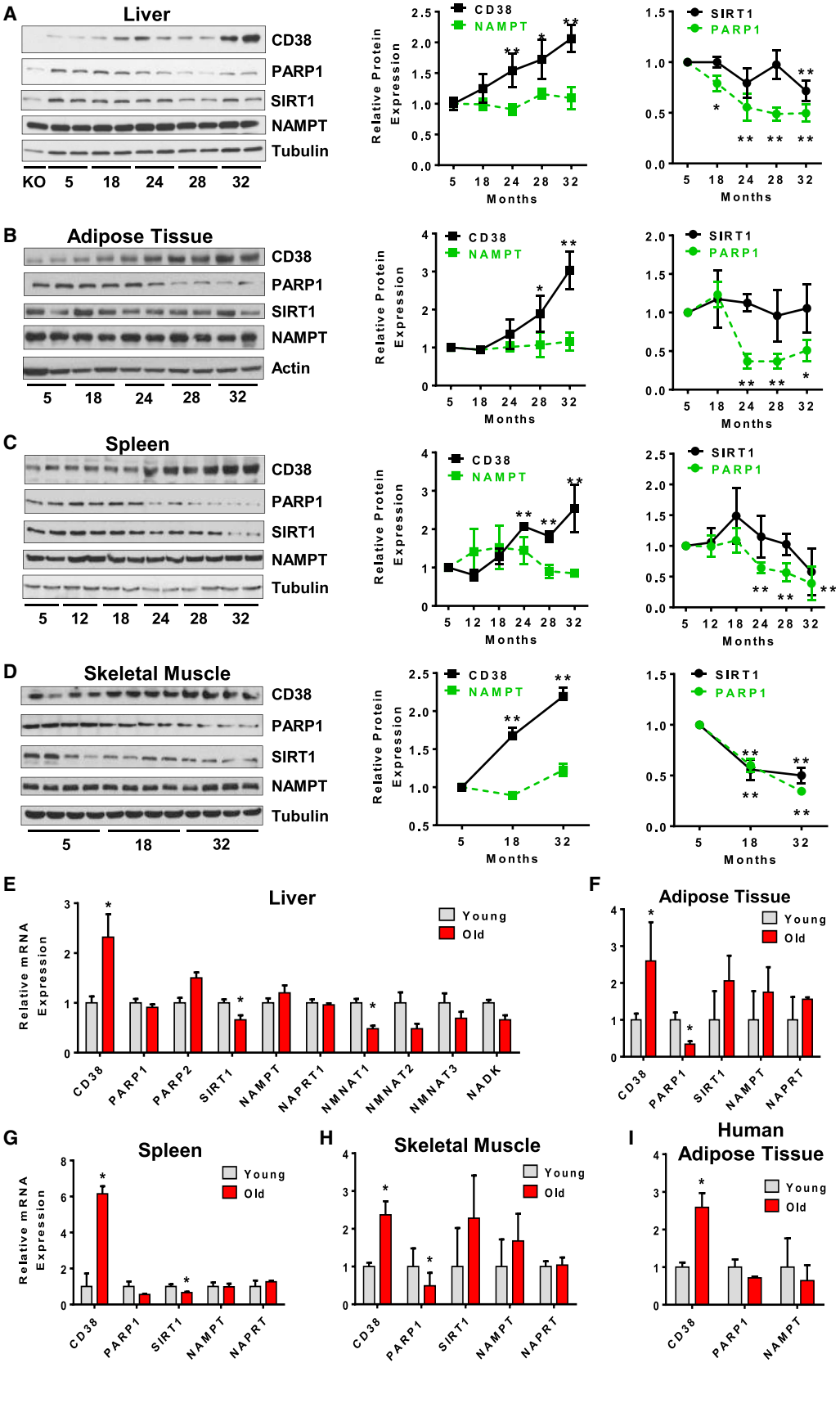

(legend on next page)

ultra-performance liquid chromatography (UPLC)-mass spectroscopy assay (see Experimental Procedures and Supplemental Information, available online) (Figures S1A–S1C). We also further optimized and validated the cycling assay, and determined that it is very specific for NAD^+ and NADH and does not detect any of the other nucleotides or NAD derivatives tested, including NADP, NAAD, NAADP, cADPR, ATP, ADP, and others (Figure S1A). The results obtained with both methods confirm that there is indeed a decrease in levels of both NAD^+ and NADH in murine tissues during chronological aging (Figures S1B and S1C). Furthermore, both techniques correlated extremely well for both nucleotides (correlation coefficient of $r = 0.95$ for NAD^+ and 0.97 for NADH; Figures S1B and S1C). In subsequent experiments, NAD levels were generally assayed using the cycling method. Because our data agree with previous studies indicating that tissue NAD levels decline with aging, we next investigated the mechanisms leading to this age-related NAD decline in tissues.

NAD decline could be caused by an increase in NAD-consuming enzymes and/or a decrease in its synthesizing enzymes. Some of the NAD-degrading enzymes in mammalian tissues include CD38, PARPs, and SIRTUINS. We have previously shown that CD38, in particular, is one of the main NAD-degrading enzymes in mammalian tissues (Aksoy et al., 2006; Barbosa et al., 2007). Furthermore, PARP1 has been proposed to be involved in NAD decline in tissues, and SIRT1 is an NAD-dependent deacetylase that plays a key role in age-related metabolic phenotypes (Bai et al., 2011; Bai and Cantó, 2012; Imai and Guarente, 2014). Thus, we first investigated the expression of these enzymes in several mouse tissues during aging. As shown in Figure 1, the protein levels of both PARP1 and SIRT1 decreased in all of the tissues tested, including liver, white adipose tissue, spleen, and skeletal muscle (Figures 1A–1D and S1D–S1F). These data indicate that the age-related NAD decline is not mediated by an increase in the expression of either PARP1 or SIRT1. In sharp contrast, levels of the NADase CD38 increased at least two to three times during chronological aging in all tissues tested, as detected by immunoblotting (Figures 1A–1D and S1D–S1F). Furthermore, in the liver, we observed that the number and intensity of CD38-positive cells increased during aging as determined by flow cytometry (Figure S1G).

We further investigated if the age-related NAD decline could be mediated by a decrease in the protein levels of NAD-synthesizing enzymes such as NAMPT and NAPRT1. Neither NAMPT nor NAPRT1 protein levels changed significantly during aging in tissues (Figures 1A–1D and S1H). All immunoblots were performed with samples obtained from 6–14 mice for each age, and several of the original gels are presented in Figure S1.

To further confirm and expand our findings, we measured the mRNA levels of these NAD-degrading and NAD-synthesizing enzymes in tissues of young (3 months old) and old mice (32 months old). Similar to protein expression, CD38 mRNA levels also increased in old mice when compared to young mice in all tissues tested (Figures 1E–1H). The increase in CD38 mRNA in tissues of old mice was about 2.5 times in liver, adipose tissue, and skeletal muscle, and up to 6 times in the spleen (Figures 1E–1H). In contrast, PARP-1 and SIRT1 mRNA expression did not change in a way that could explain the age-related NAD decline in any of the tissues tested (Figures 1E–1H). In fact, in the case of PARP1, mRNA levels actually declined significantly in several tissues (Figures 1F–1H). As for the NAD-synthesizing enzymes, the mRNA levels for neither NAMPT nor NAPRT decreased in any of the tissues during aging (Figures 1E–1H). We also analyzed the mRNA expression of additional NAD-degrading and NAD-synthesizing enzymes in the liver of young and old mice (Figure 1E). Expression of the enzymes NMNAT1–NMNAT3 was lower in older mice, but a significant difference was observed only for NMNAT1 (Figure 1E).

To determine if the increase in CD38 expression observed in mice could also be present in humans, we measured the mRNA expression of some of the key enzymes involved in NAD metabolism in human adipose tissue from young (average age 34) and old (average age 61) subjects. Akin to mouse tissues, the expression of CD38 increased up to 2.5 times in fat tissue obtained from older subjects when compared to younger subjects (Figure 1I). In contrast, levels of neither PARP1 nor NAMPT changed significantly with aging in these samples (Figure 1I).

CD38 Plays a Key Role in the Age-Related NAD Decline

Our data together show that CD38 protein and mRNA expression increase during aging in multiple tissues, and indicate that this enzyme could play a major role in age-related NAD decline. To determine if these changes in expression were associated with an increase in NAD^+-degrading activity, we first measured CD38 NADase activity in tissues from mice at different ages. Consistent with CD38 mRNA and protein expression results, CD38 enzymatic activity also increased during aging in liver, white adipose tissue, spleen, and skeletal muscle (Figure 2A). We also expanded our observations and determined that the

Figure 1. CD38 Expression Increases with Aging

(A) Immunoblots for CD38, PARP1, SIRT1, NAMPT, and Tubulin in mice liver (left). On the right, graphs show relative protein expression of SIRT1, PARP1, CD38, and NAMPT. Relative expression of each protein was calculated as a ratio to Tubulin levels in each lane, and then calculated relative to 5-month-old mice ($n = 12$ for each age, $^*p < 0.05$, $^{**}p < 0.01$). In the experiments of (A)–(H), animals were obtained from the NIA aging colony.

(B–D) Immunoblots for CD38, PARP1, SIRT1, NAMPT, and Tubulin in mice adipose tissue (B), spleen (C), and skeletal muscle (D) (left). On the right, graphs show relative protein expression of SIRT1, PARP1, CD38, and NAMPT in the tissues. Relative expression of each protein was calculated as a ratio to Tubulin in each lane, and then calculated relative to 5-month-old mice ($n = 4$–6 for each age, $^*p < 0.05$, $^{**}p < 0.01$).

(E) Relative mRNA levels of CD38, PARP1, PARP2, SIRT1, NAMPT, NAPRT1, NMNAT-1, NMNAT-2, NMNAT-3, and NADK in liver of young and old mice (3 and 32 months of age, respectively). ($n = 4$ animals for each age, $^*p < 0.05$, versus 3-month-old mice).

(F–H) Relative mRNA levels of CD38, PARP1, PARP1, SIRT1 NAMPT, and NAPRT1 in adipose tissue (F), spleen (G), and skeletal muscle (H) (3 and 32 months of age, respectively) ($n = 4$ animals for each age, $^*p < 0.05$, versus 3-month-old mice).

(I) Relative mRNA levels of CD38, PARP1, and NAMPT in omental adipose tissue of human subjects with average ages of 34 (young) and 61 (old) ($n = 9$ for each age, $^*p < 0.05$, versus young group).

All values are mean ± SEM.

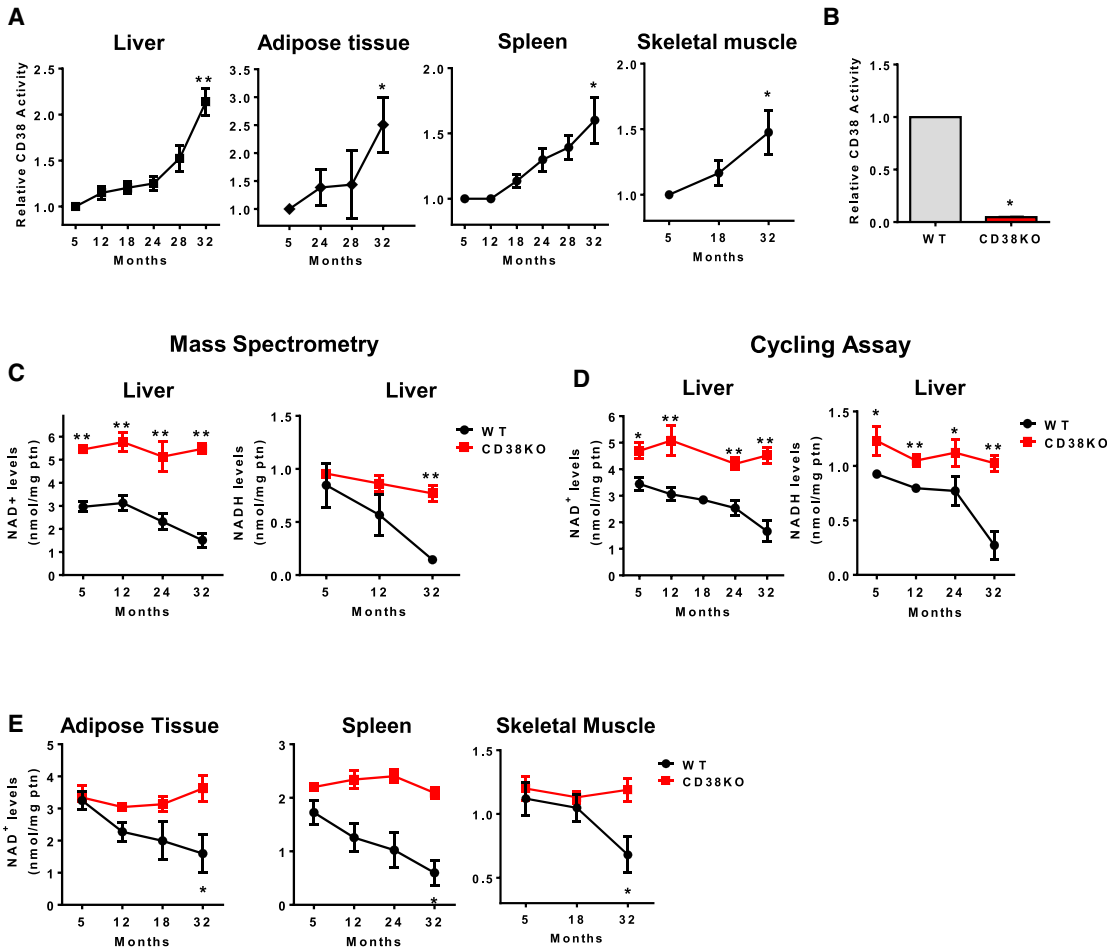

Figure 2. CD38 Regulates the Age-Related NAD$^+$ Decline

(A) CD38 activity in liver, adipose tissue, spleen, and skeletal muscle of aging mice (n = 6 animals for each age, **p < 0.01, versus 5-month-old mice).

(B) CD38 activity in liver of 1-year-old WT and CD38KO litter mate mice (*p < 0.05).

(C) Total liver NAD$^+$ and NADH levels in WT and CD38KO mice during aging measured by mass spectroscopy (n = 4 mice for each age, *p < 0.05, **p < 0.01, versus 5-month-old mice).

(D) Total liver NAD$^+$ and NADH levels in WT and CD38KO mice during aging measured by cycling assay (n = 14 animals for each age, *p < 0.05, **p < 0.01, versus 5-month-old mice).

(E) NAD$^+$ levels in adipose tissue, spleen, and skeletal muscle of WT and CD38KO mice during aging (n = 4 animals for each age, *p < 0.05, **p < 0.01, versus 5-month-old mice).

All values are mean ± SEM.

CD38 NADase activity also increased at least 50% in the ilium, jejunum, and kidney during the aging process (Figure S2A). Our control experiments with CD38KO mice confirm the specificity of the NADase assay for CD38 (Figure 2B). In fact, we did not detect significant NADase activity in any of the CD38KO tissues tested.

Interestingly, when CD38 activity or protein expression was plotted against NAD$^+$ decline in aging, an excellent inverse correlation coefficient was observed ($r = -0.95$ and $r = -0.99$, respectively; Figure S2B). These results indicate that an increase in CD38 protein expression and activity during aging could be the cause of the age-related NAD$^+$ decrease. The same was not observed for PARP1 (Figure S2C). Consistent with a decrease in PARP1 protein expression, levels of PARylated proteins declined in the liver of aged mice (Figure S2D). This decrease in PARylation correlated positively with a decrease in both PARP1 protein expression and tissue NAD$^+$ levels (Figure S2E). These findings indicate that the decline in PARylation was potentially a consequence of a decrease in either NAD$^+$ or PARP1 levels, and do not support a causal role for PARP1 in the age-related NAD$^+$ decline.

To further demonstrate that CD38 is the main enzyme regulating NAD levels, we examined the role of all three NAD$^+$-degrading enzymes, CD38, PARP1, and SIRT1, in maintaining NAD$^+$ levels in cells. First, we measured NAD$^+$ levels in mouse embryonic fibroblasts (MEFs) derived from wild-type (WT), CD38, PARP1, and SIRT1 KO mice. Only CD38KO MEFs showed a significant increase in cellular NAD$^+$ levels when compared to WT cells (Figures S2F–S2H). PARP1KO MEFs showed a trend for an increase in NAD$^+$, but it did not reach

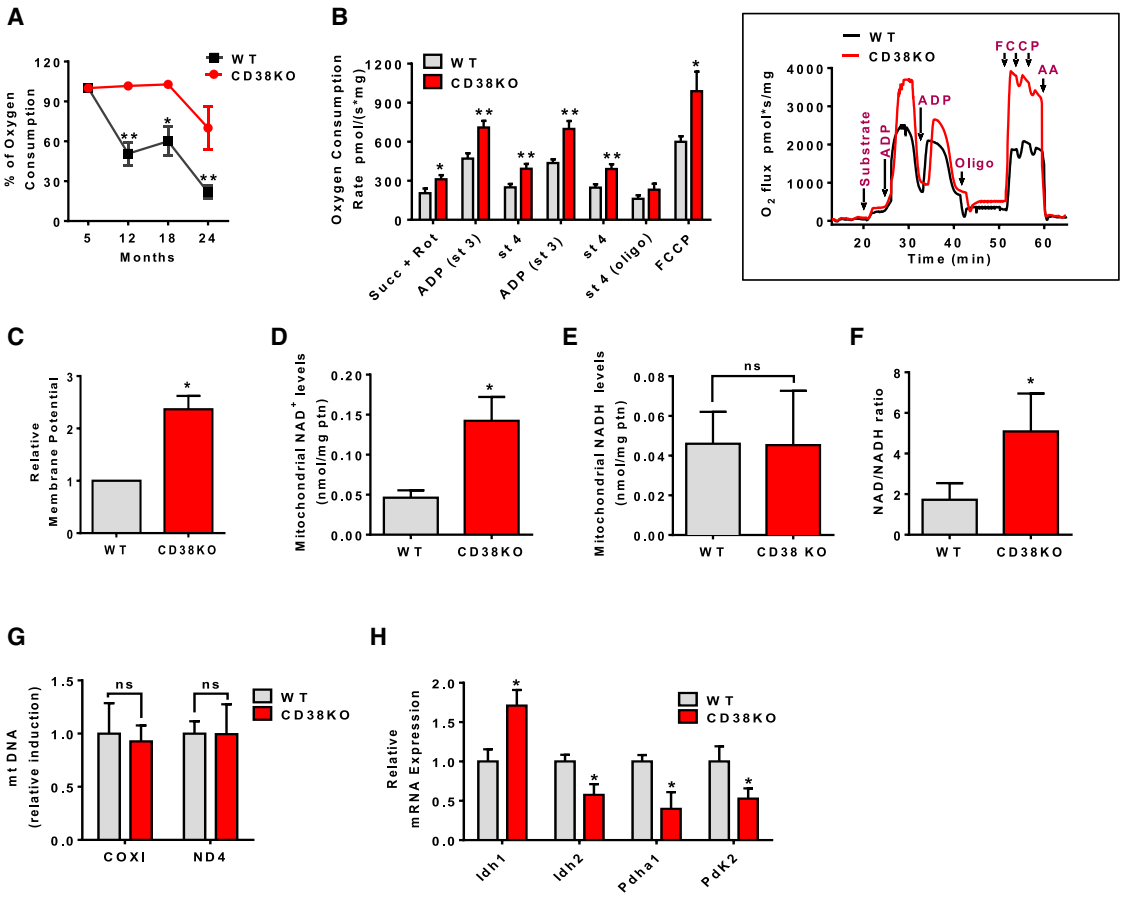

Figure 3. CD38 Deficiency Upregulates Mitochondrial Function and Increases NAD$^+$/NADH Ratio in Mitochondria

Liver of WT and CD38KO 12-month-old litter mate mice were used for the measurements below in (B)–(H). All values are mean ± SEM.

(A) Percentage of oxygen consumption coupled to ATP synthesis in isolated mitochondria during aging in WT and CD38KO mice (n = 4 animals for each age, *p < 0.05, **p < 0.01, versus 5-month-old mice).

(B) Oxygen consumption rates in isolated mitochondria. The following drugs were added for the experimental profile: 10 mM succinate and 1 μM rotenone (Succ + Rot), 0.15 mM ADP, 1 μg/mL oligomycin (Oligo), and 1 μM FCCP (inset) (n = 4, *p < 0.05, **p < 0.01, versus WT mice).

(C) Relative membrane potential in mitochondria (*p < 0.05 versus WT mice).

(D–F) Total NAD$^+$ levels (D), NADH levels (E), and the NAD$^+$/NADH ratio (F) in isolated mitochondria (n = 3, *p < 0.05 versus WT mice).

(G) Relative mtDNA quantification of COX I and ND4 as mitochondrial-encoded genes normalized by GAPDH.

(H) Relative mRNA expression of glucose metabolism pathway enzymes (n = 6, *p < 0.05 versus WT mice).

statistical significance (Figure S2H). We further tested the role of CD38 and PARP1 in regulating NAD$^+$ levels in vivo, using 1-year-old WT, CD38, and PARP1KO mice (Figures S2I and S2J). In agreement with the data in cells, CD38KO had higher NAD$^+$ levels than both WT and PARP1KO in all tissues tested. In contrast, although there was a trend for an increase in NAD$^+$ in the liver and adipose tissue of PARP1KO mice, no statistical significant difference was observed between WT and these mice (Figure S2J). To directly test the hypothesis that CD38 was responsible for the age-related NAD decline, we measured NAD levels in tissues from WT and CD38KO mice at various ages. Consistent with our hypothesis, we observed that although NAD$^+$ levels declined significantly during chronological aging in all WT tissues, they were stable in CD38KO mice (Figures 2C–2E). In sharp contrast, in CD38KO mice NAD levels remained constant at all ages (Figures 2C–2E). In the liver, in particular, neither NAD$^+$ nor NADH levels significantly decline in CD38KO mice (Figures 2C and 2D). These results were observed using both the cycling and the UPLC-mass spectroscopy assays (Figures 2C and 2D), and demonstrate for the first time that CD38 has a major role in regulating NAD levels during the aging process.

CD38 Regulates Mitochondrial Function in Mammalian Tissues during Aging

Mitochondrial function decline is a hallmark of aging (Gomes et al., 2013; Lanza and Nair, 2010), and cellular NAD$^+$ decline has been implicated as a potential cause of this age-related mitochondrial dysfunction. Here we investigated the role of CD38 in the development of mitochondrial dysfunction during the aging process in liver tissue. First, we observed that the respiration-driving ATP synthesis decreases almost 70% in WT liver mitochondria (LM) during aging (Figure 3A), and this decrease correlated positively with the age-related decrease

in NAD^+ levels (r = 0.952; Figure S3A). In agreement with the role of CD38 in the age-related NAD^+ decrease, the decline in mitochondrial function was forestalled in CD38KO mice (Figure 3A).

Oxygen consumption rates in LM were at least 2.5 times higher in all respiratory states in 1-year-old CD38KO mice compared to WT mice, irrespective of the substrate used (Figure 3B; Table S1). Similar results were also observed in mitochondria isolated from spleen of 1-year-old mice (Table S2) or in LM from 2-year old mice submitted to normal or high-fat diet (Figures S3B–S3E). These results, together with the higher mitochondrial membrane potential observed in 1-year-old CD38KO mice (Figure 3C), confirm the increased mitochondrial activity in these animals. Higher levels of NAD^+ and NAD^+/NADH ratio were also detected in the mitochondria of 1-year-old CD38KO mice (Figures 3D–3F). Thus, we propose that chronic increases in cellular NAD levels in CD38KO mice also lead to increases in NAD in cellular compartments such as mitochondria.

To further explore the role of CD38 in mitochondrial function, we measured the expression of mtDNA and of the mRNA of mitochondrial enzymes. mtDNA copy number was not significantly different between 1-year-old WT and CD38KO (Figure 3G), suggesting that the number of mitochondria was not altered in liver of CD38KO mice. This observation was further supported by the relative expression of genes involved in mitochondrial biogenesis such as PPAR-γ, PGC1α, and NRF1 in liver from 1-year-old WT and CD38KO mice (Figure S3F). Interestingly, we found that mRNA levels of Pdha1 and PDK2 that are involved in pyruvate entrance into mitochondria were decreased in CD38KO mice (Figure 3H). We also found a decrease in mRNA expression levels in glycolytic/pentose pathway enzymes and small solute carriers in LM of 1-year-old CD38KO mice compared to WT mice (Figure S3G). These changes may be compensatory to an increase in mitochondrial oxidative capacity and mitochondrial NAD levels. Our results in animals indicate that there is an increase in oxygen consumption in CD38KO mice, which is related to an increase in mitochondrial NAD, and not mitochondrial biogenesis.

Changes in CD38 Expression in Cells Regulate Mitochondrial Function

To confirm the role of CD38 in the regulation of mitochondrial function, oxygen consumption experiments were performed in intact cells after transfection with a CD38 plasmid. Expression of CD38 in 293T cells transfected with a control vector was nearly absent (Figure 4A). Cells that were transfected with CD38 plasmid displayed high CD38 expression and NADase activity and lower NAD^+ and NADH levels in whole cells (Figures 4B–4D). Next, we measured the respiratory capacity in intact cells and observed that CD38 transfection induced a severe decrease in total respiratory capacity and caused a higher lactate release when compared with vector-transfected cells (Figures 4E and 4F). Our results show that an increase in CD38 expression in cells leads to mitochondrial metabolic dysfunction, and likely to an increase in dependence on glycolysis. We further evaluated the status of the mitochondria in these cells. Electron microscopy shows a very significant abnormal mitochondrial morphology, such as lost and swollen cristae, and other morphological abnormalities in CD38-overexpressing cells (Figures 4G and S4). It has been shown that cellular stress can induce the opening of the mitochondrial transition pore, causing swelling of the mitochondria, loss of membrane potential, and leakage of mitochondrial matrix components such as NAD and NADH (Di Lisa et al., 2001). Thus, to test the "health" status and integrity of the mitochondria in CD38-overexpressing cells, we isolated mitochondria and measured the content of mitochondrial NAD^+ and NADH. We observed a severe loss of NAD^+ and NADH in isolated mitochondria from CD38-overexpressing cells (Figure S4I). It is possible that this could be due to degradation via CD38, and/or leakage of these nucleotides from dysfunctional mitochondria either in situ or during the mitochondrial isolation.

We further speculated that the severe mitochondrial dysfunction caused by overexpression of CD38 in cells would lead to a compensatory mitochondrial biogenesis. In fact, both the mtDNA/genomic DNA ratio and citrate synthase activity were higher in cells expressing CD38 than vector-transfected cells (Figures 4H and 4I). These data suggest that in our overexpression experiments, the decline in cellular NAD levels may cause metabolic dysfunction mediated by intrinsic changes in the mitochondrial machinery, with a "reactive" compensatory mitochondrial biogenesis.

To determine the role of endogenous CD38 in cells, we also performed experiments knocking down CD38 in A549 cells. A549 cells express detectable levels of CD38, and transfection with a CD38 short interfering RNA (siRNA) significantly decreased expression of CD38 and NADase activity, in comparison to control siRNA-transfected cells (Figure 4J). Furthermore, in CD38 siRNA-transfected cells, both NAD^+ levels and total respiratory capacity were higher than in control siRNA-transfected cells (Figures 4K and 4L), confirming that changes in endogenous CD38 expression levels regulate NAD and mitochondrial function.

CD38 Regulates Metabolic State by an SIRT3-Dependent Mechanism

SIRT3 is one of the sirtuins localized in mitochondria that regulate key mitochondrial proteins important for metabolism and oxidative homeostasis such as LCAD, IDH2, SDH, and MnSOD (Finley et al., 2011; Hirschey et al., 2010; Shimazu et al., 2010; Tao et al., 2010; Yu et al., 2012). To determine if CD38 regulates the NAD^+-dependent SIRT3 activity and mitochondrial protein lysine acetylation in vivo, we analyzed the profile of acetylated proteins in mitochondria from 1-year-old WT and CD38KO livers. Although levels of mitochondrial SIRT3 were similar, levels of acetylated proteins were considerably higher in WT than CD38KO LM (Figures 5A and S5A). In addition, SIRT3 activity in the presence of endogenous NAD^+ in the liver tissue was 3.5 times higher in CD38KO than WT mice (Figure 5B). In contrast, when saturating levels of exogenous NAD^+ were added to the enzymatic assay, similar SIRT3 activities were observed between WT and CD38KO (Figure 5B). These data together indicate that by changing cellular NAD^+, CD38 controls SIRT3 activity without changes in SIRT3 levels.

To address the role of SIRT3 in the mitochondrial metabolic profile observed in CD38KO mice, we generated CD38/SIRT3 double KO mice on a C57BL6/129 s background and used the derived F3 generation of these crosses. As expected, livers of

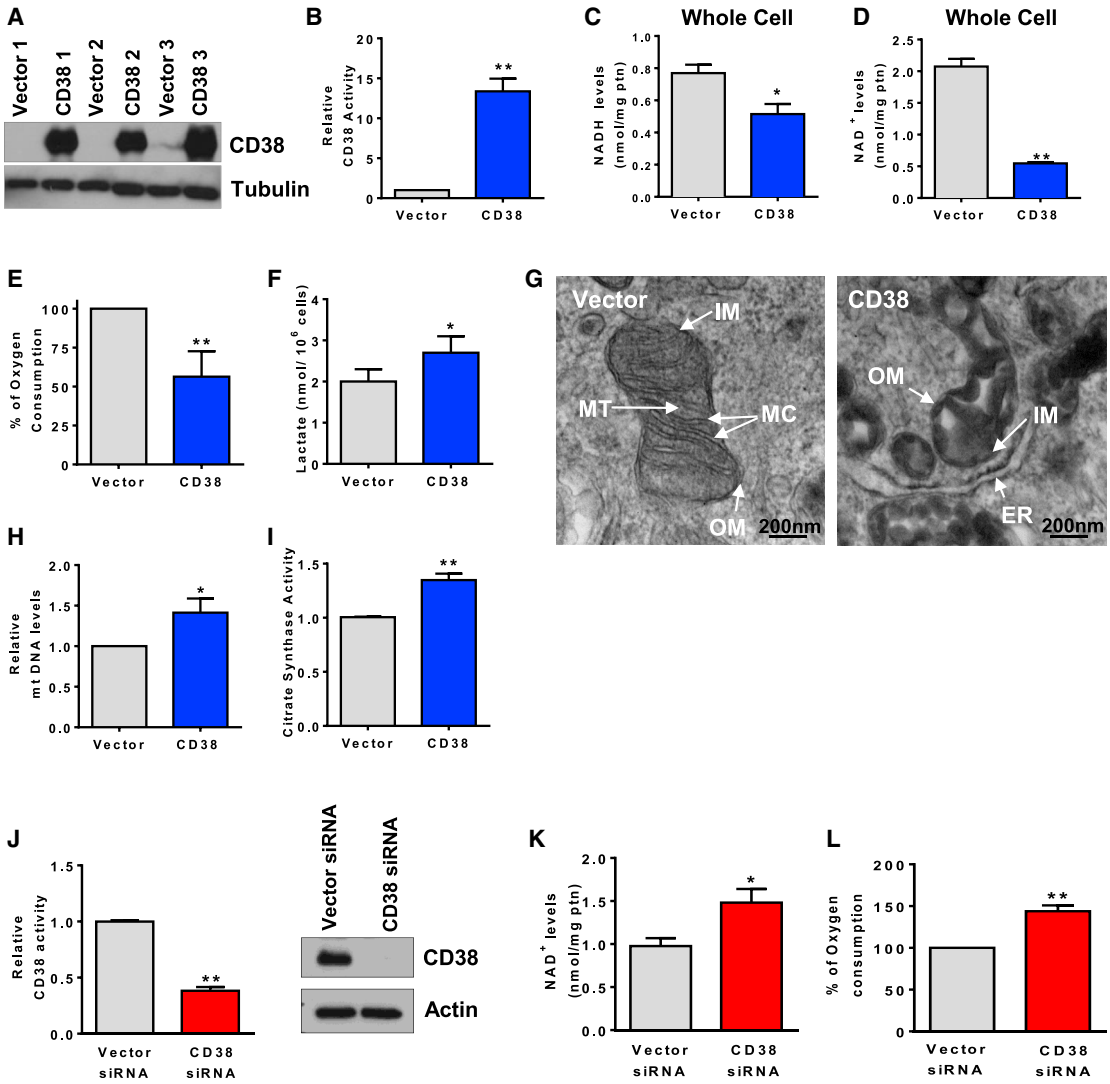

Figure 4. Changes in CD38 Expression Regulate NAD$^+$ levels and Mitochondrial Function in Cells

293T cells expressing vector or Flag.CD38 were used in experiments (A)–(I) and A549 cells were used in (J)–(L). All values are mean ± SEM. *$p < 0.05$, **$p < 0.01$, compared to control cells.

(A) Immunoblotting for CD38 and Tubulin.

(B) CD38 NADase activity (n = 5).

(C and D) Total NAD$^+$ (C) and NADH (D) levels in whole cells (n = 5).

(E) Mitochondrial oxygen consumption in intact cells. Histogram represents the percent oxygen consumption under FCCP-induced maximum respiration (n = 6).

(F) Lactate released in media (n = 5).

(G) Transmission electron microscopy. Scale bar, 200 nm. OM, outer membrane; IM, internal membrane; MT, mitochondrial matrix; MC, mitochondrial cristae; ER, endoplasmic reticulum.

(H) Relative mtDNA quantification (n = 4).

(I) Citrate synthase activity (n = 9).

(J) CD38 NADase activity (n = 5) and immunoblotting for CD38 and Tubulin.

(K) Total NAD$^+$ levels (n = 5).

(L) Routine oxygen consumption (n = 3).

both 2-year-old CD38KO and CD38/SIRT3KO mice have higher mitochondrial NAD$^+$ levels compared to WT mice (Figure 5C). Interestingly, mitochondrial NAD$^+$ was slightly higher in the double KO compared to the CD38KO (Figure 5C). This may indicate a lower utilization of mitochondrial NAD$^+$ in the absence of both CD38 and SIRT3. We further performed a glucose tolerance test and determined the mitochondrial function in these 2-year-old mice. CD38KO mice have an improved glucose tolerance profile compared to WT and SIRT3KO, which is reversed in the CD38/SIRT3KO mice (Figure 5D).

At 2 years of age, CD38KO mice had an increased oxygen consumption coupled to ATP synthesis over WT that was reverted in

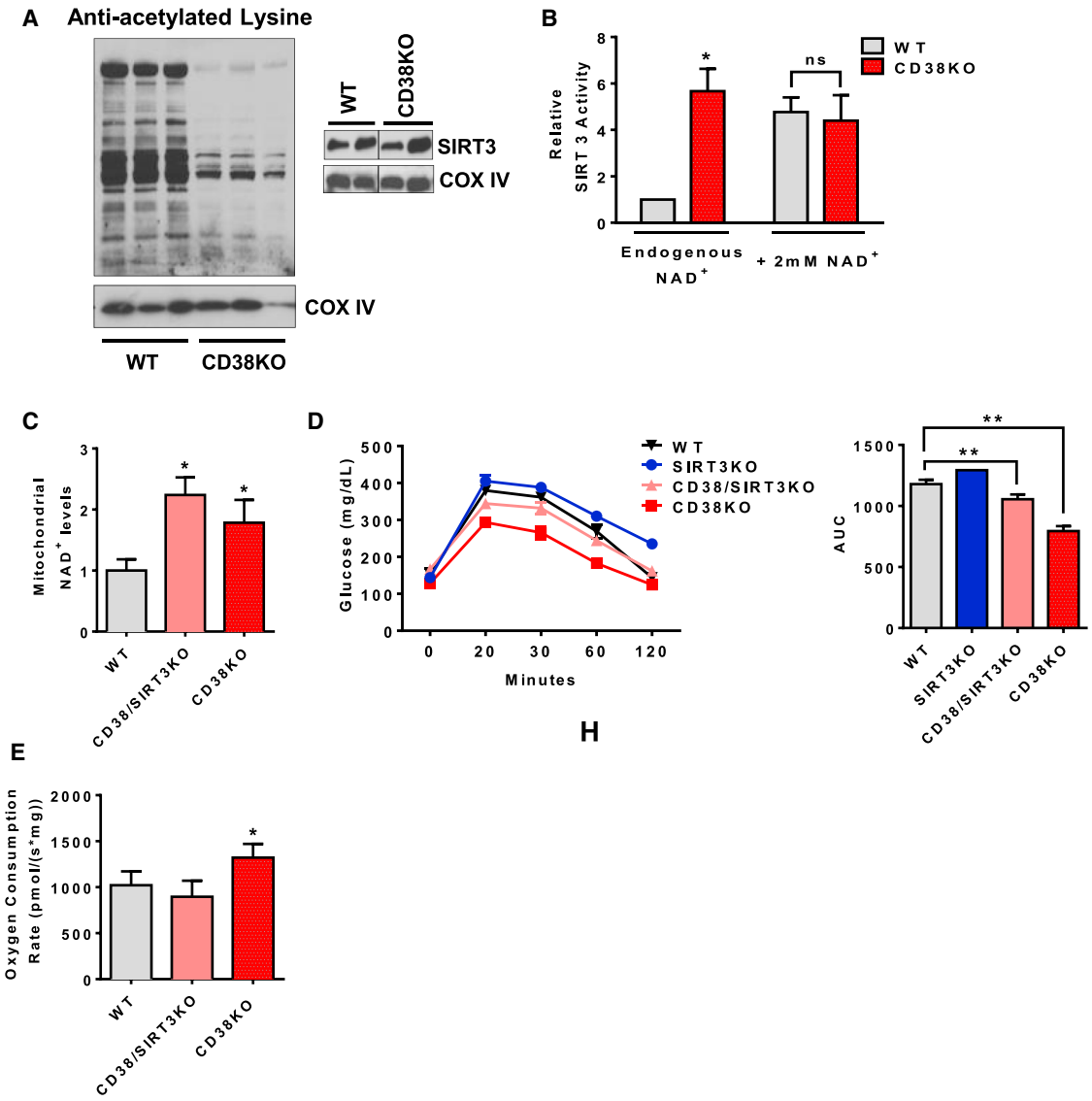

Figure 5. CD38 Controls the Metabolic Response in Aged Mice by Activating SIRT3-Dependent Mechanisms

(A) Mitochondrial protein acetylation profile (upper panel) and immunoblotting for SIRT3 in 1-year-old WT and CD38KO litter mate mice (lower panel). Each lane represents one independent mouse.

(B) SIRT3 activity in LM isolated from 1-year-old WT and CD38KO litter mate mice with endogenous contaminant NAD^+ or addition of a saturating dose of 2 mM NAD^+ (n = 4, *p < 0.05; ns, non-significant; p > 0.05 versus WT control).

(C) NAD^+ levels in isolated LM from 2-year-old litter mate WT, CD38KO, and CD38/SIRT3KO mice (n = 6, *p < 0.05 versus WT mice).

(D) Glucose concentration in 2-year-old litter mate WT, SIRT3KO, CD38KO, and CD38/SIRT3KO mice after i.p. injection of glucose (left graphs). Area under the curve for glucose concentrations in different mice (right graphs) (n = 8, **p < 0.01, *p < 0.05, versus WT mice).

(E) Oxygen consumption rates coupled to ATP synthesis in LM isolated from 2-year-old litter mate WT, CD38KO, and CD38/SIRT3KO mice (n = 6, *p < 0.05 versus WT mice).

All values are mean ± SEM.

the CD38/SIRT3KO mice (Figure 5E). We also determined that ablation of SIRT3 in CD38KO mice abrogated the protection against high-fat-diet-induced obesity and glucose intolerance that we have previously described in 1-year-old mice (Figures S5B and S5C; Barbosa et al., 2007). These results suggest that metabolic and mitochondrial function is positively regulated in CD38KO mice by a pathway that requires not only increases in NAD^+ levels, but may also require the enzyme SIRT3.

CD38 Degrades NAD^+ Precursors: Implications for NAD^+ Replacement Therapy

NAD^+ precursors such as NMN and NR (nicotinamide riboside) have been proposed as NAD^+-replacement therapy for age- and diet-induced metabolic dysfunction (Cantó et al., 2012; Gomes et al., 2013; Imai and Guarente, 2014; Prolla and Denu, 2014; Yoshino et al., 2011). Recombinant CD38 has been shown to hydrolyze NMN in vitro (Grozio et al., 2013), as confirmed here

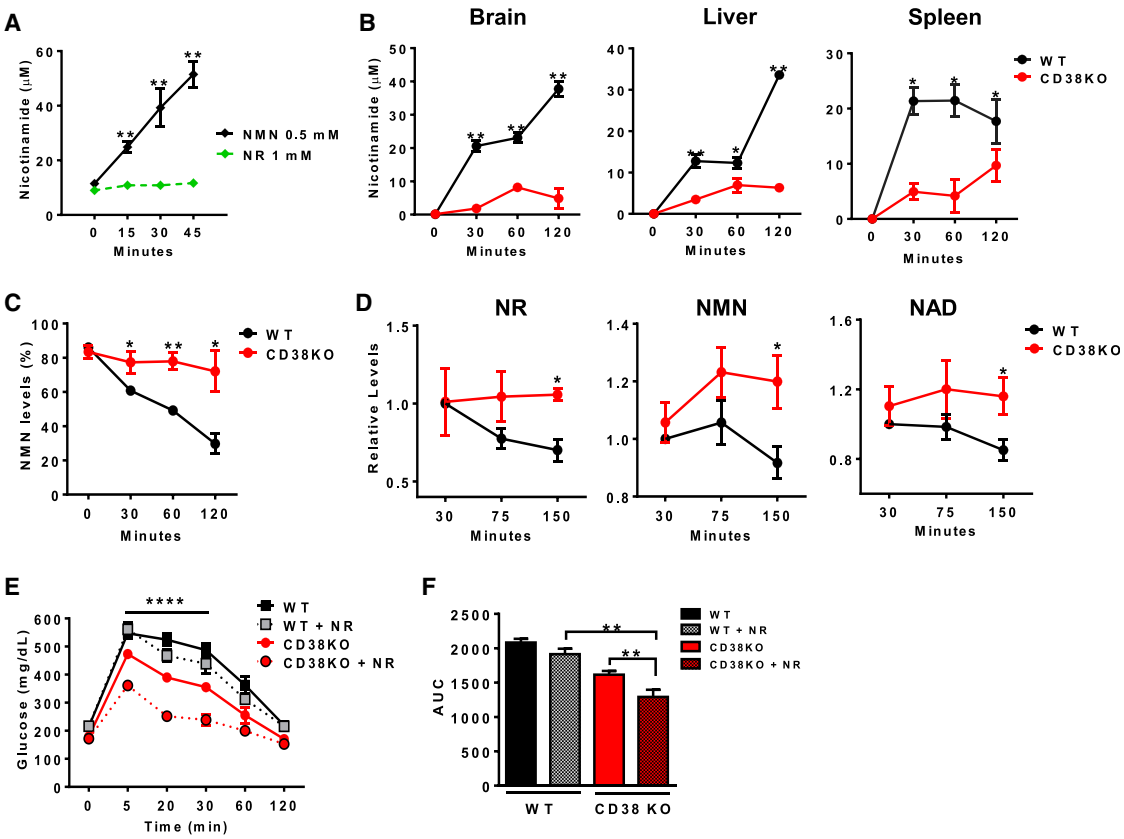

Figure 6. CD38 Regulates the NR-Induced Metabolic Improvement in High-Fat Diet

(A) Nicotinamide concentration in vitro after incubation of 1 mM NR or 0.5 mM NMN with CD38 recombinant protein. The metabolites were measured by HPLC (n = 3, **p < 0.01 versus NMN incubation).

(B) Nicotinamide concentration in different tissue homogenates from WT and CD38KO mice after incubation with 1 mM NMN. The metabolites were measured by a coupled assay (n = 3,*p < 0.05, **p < 0.01, versus WT mice).

(C) Nicotinamide concentration in blood from WT and CD38KO mice after incubation with 1 mM NMN. The metabolites were measured by HPLC (n = 3, *p < 0.05, **p < 0.01, versus WT mice).

(D) Levels of NR, NMN, and NAD in blood of WT and CD38KO mice after i.p. injection of 500 mg/kg NR. The metabolites were measured by HPLC (n = 3, *p < 0.05 versus WT mice). Due to the technique used, it is possible that the NR peak in the figure could contain other metabolites.

(E and F) Glucose concentration in WT and CD38KO mice after 16 weeks of high-fat diet, treated with 500 mg/Kg nicotinamide riboside (NR) (dotted line) intraperitoneally. The controls received PBS injection (solid line)

(E) Two-way ANOVA and Bonferroni's post-test with repeated measures show significant interaction between the glucose curve for CD38KO and CD38KO + NR (****p < 0.0001).

(F) Quantification of glucose area under the curve (**p < 0.01, n = 10).

All values are mean ± SEM.

by us (Figure 6A). However, it has not been demonstrated whether CD38 has a role in the degradation of these compounds in vivo. We now report, for the first time, that CD38 is one of the main enzymes degrading NMN in mouse tissues (Figure 6B), implying that CD38 has a key role in the pharmacokinetics of NMN. This was confirmed by the rapid disappearance of NMN in blood of WT, but not CD38KO, mice (Figure 6C). Due to the rapid degradation of NMN, we performed further in vivo experiments with NR as an NAD^+ precursor. NR is resistant to CD38 enzymatic activity in vitro (Figure 6A). However, since NR is converted to NMN (Bieganowski and Brenner, 2004; Grozio et al., 2013), it is still possible that CD38 may have a role in NR-mediated pharmacokinetics. To test this hypothesis, we administered NR to WT and CD38KO mice and followed plasma levels of NR, NMN, and NAD^+. We show that following an intraperitoneal (i.p.) injection of NR (500 mg/kg), the levels of NR, NMN, and NAD^+ in the blood of CD38KO mice are more stable than in WT animals (Figure 6D). In fact, levels of NR rapidly decline in WT mice, with a decrease of about 25% in the first 75 min, while NR levels are maintained in CD38KO mice. A total of 150 min after NR injection, there were still higher levels of NMN and NAD^+ in plasma of CD38KO than in WT mice (Figure 6D). These results indicate that CD38 is involved in the metabolism of NAD precursors in vivo. To further explore the role of CD38 in NAD-replacement therapy in vivo, we selected 2-year-old C57BL/6 WT and CD38KO mice that had similar normal glycemia, and induced glucose intolerance with high-fat diet. After 16 weeks of high-fat diet, WT mice become severely glucose intolerant, and although CD38KO were somewhat resistant to the effects of the diet, they still developed a significant degree of glucose

intolerance (Figures S6A and S6B). At the end of 16 weeks, we gave an i.p. injection of NR and determined its effect in glucose tolerance tests. Consistent with a role of CD38 in NR-mediated NAD^+ replacement therapy, a single dose of NR was able to ameliorate glucose intolerance only in CD38KO mice (Figures 6E and 6F). These results confirm that CD38 has the ability to influence NAD^+-replacement therapy in vivo. We propose that NAD replacement-based therapies with NMN and NR for metabolic dysfunction could be significantly improved by combination with CD38 inhibitors.

DISCUSSION

The mechanisms that lead to age-related metabolic dysfunction have not been elucidated. Recently, a growing body of evidence indicates that cellular NAD^+ levels decrease during the aging process in both rodents and humans (Zhu et al., 2015; Gomes et al., 2013; Braidy et al., 2011; Scheibye-Knudsen et al., 2014, Massudi et al., 2012). Our first goal here was to confirm these findings. We used two different methods to measure NAD levels in mouse tissues and clearly demonstrate that aging mice experience a sharp decrease in tissue NAD levels that positively correlates with a decrease in mitochondrial function. Thus, our next goal was to understand the mechanisms that lead to this age-related NAD decline and metabolic dysfunction.

One of the current hypotheses to explain the age-related NAD decline is that this phenomenon could be mediated by accumulation of DNA damage and activation of PARP1 during aging (Bai and Cantó, 2012; Imai and Guarente, 2014). However, there is no consensus about the role of PARPs in the aging process, and the concept of a deleterious increase in PARP activity during aging is controversial. In fact, it has been previously observed that levels of PARPs may either decrease or increase with aging (Bakondi et al., 2011; Beneke et al., 2010; Noren Hooten et al., 2012; Zhang et al., 2014). Furthermore, based on the disposable soma evolutionary aging hypothesis, it is expected that the aging organism would present limited repair mechanisms and not necessarily an increase in damage inputs or repair machinery (Kirkwood and Rose, 1991). In fact, in the disposable soma theory, it has been proposed that to optimize energy use, biological systems may invest most of their energy in growth and development and little in damage control and repair. In support of this idea, our data indicate that PARP1 levels actually decrease in all mouse tissues tested during the aging process. Thus, we postulated that other NAD-degrading mechanisms besides PARP1 activation are responsible for the age-related NAD^+ decline.

We explored the role of the NADase CD38 in NAD decline in several tissues of aging mice. We clearly demonstrate that CD38 levels increase in mouse tissues during aging, and that CD38 is directly involved in the process that mediates the age-related NAD^+ decline. Our experiments were comprehensive and included multiple tissues and techniques, and we demonstrated that CD38 protein, mRNA, and NADase activity increased during aging. Although further experiments are necessary to translate our findings to humans, we have also observed an increase in CD38 mRNA expression in white adipose tissue derived from older humans compared to younger subjects. Interestingly, in support of our findings, CD38/NADase activity has been proposed to increase in the blood of aging human subjects (Polzonetti et al., 2012). In addition, we have recently shown that stable overexpression of CD38 in cancer cells leads to the development of features of cellular senescence (Chini et al., 2014).

Our current studies further provide evidence that an increase in CD38 in aging mice correlates with the development of mitochondrial dysfunction. The effects of CD38 on mitochondrial function may be mediated, at least in part, by modulation of the availability of NAD^+ as a substrate to mitochondrial enzymes, including SIRT3. However, since CD38 regulates both global cellular and mitochondrial NAD levels, we cannot exclude the possibility that the effect of CD38 may be mediated by interference in many of the other cellular NAD^+-dependent processes, including oxy-reduction reactions, signaling, and epigenetics.

Our studies raise several new important questions that need to be addressed to understand the precise mechanisms leading to age-related NAD^+ decline. One question, for example, concerns what the signaling mechanisms are that lead to CD38 accumulation in tissues during the aging process. We and others have previously shown that lipopolysaccharides (LPSs) and inflammatory cytokines such as TNF-α are potent inducers of CD38 expression in cells (Barata et al., 2004; Lee et al., 2012). Interestingly, it has been proposed that during the aging process, there is an increase in levels of endotoxins and cytokines (Kim et al., 2016; Ghosh et al., 2015). Therefore, one possibility is that pro-inflammatory agents such as endotoxins may be the main drivers of the age-related increase in CD38 expression.

A second important question concerns which cells in the tissue express CD38 during aging. Since CD38 is highly expressed in inflammatory cells, it is possible that the low-grade inflammation occurring during aging may lead to an increase in the expression of CD38 in inflammatory cells and accumulation of CD38-positive inflammatory cells in the tissue.

Yet another key topic is if the CD38 ectoenzymatic activity is sufficient to explain its role as a regulator of cellular NAD^+ levels in vivo during the aging process. In addition, we do not know if the small fraction of CD38 localized in intracellular compartments can explain its role in the regulation of NAD levels in vivo. Interestingly, CD38 is a type II plasma membrane enzyme with the majority of its catalytic activity facing the outside of the cell. However, CD38/NADase has been shown to be present in intracellular organelles, including the nuclei and the mitochondria (Sun et al., 2002; Yamada et al., 1997; Aksoy et al., 2006). At this point, it is not clear if the biological effects of CD38 in NAD^+ metabolism are exclusively mediated by its extracellular or intracellular NADase activity. The fact that CD38 metabolizes not only NAD, but also NMN, may indicate that CD38 could at least in part decrease the availability of extracellular and intracellular NAD precursors to cells during the aging process.

In conclusion, we present strong evidence that CD38 is a key enzyme involved in the age-related NAD^+ decline. The recent development of potent and specific CD38 inhibitors (Escande et al., 2013; Haffner et al., 2015), together with the novel findings highlighting the role of NAD^+-replacement therapy and CD38 in age-related diseases such as hearing loss and Alzheimer's (Prolla and Denu, 2014; Chini, 2009; Blacher et al., 2015), indicate that CD38 inhibition combined with NAD precursors may serve as a potential therapy for metabolic dysfunction and age-related diseases.

EXPERIMENTAL PROCEDURES

Animal Studies

CD38KO, SIRT3KO, and PARP1KO mice were bred in our animal facility or purchased from Jackson Laboratories. SIRT3/CD38 double KO mice were generated through heterozygous breeding (see Supplemental Information for details). Studies were performed in male animals at 3–32 months of age. Mice received standard chow ad libitum, except for high-fat diet feeding experiments in which an adjusted calorie diet, 42% from fat, was given (TD.88137, Harlan Laboratories, Inc.). Fasted glucose levels and glucose tolerance were assessed as described before (Escande et al., 2013). For glucose tolerance tests, mice were fasted for 15 hr, and 50% dextrose (1.5 g/kg body weight) was injected intraperitoneally. For NR studies, mice were given a single dose (500 mg/kg body weight) by i.p. injection. Experiments were approved by the Institutional Animal Care and Use Committee (Protocol no. A52112) and adhered to the NIH Guide for the Care and Use of Laboratory Animals. C57BL/6 tissues used in some of the western blot of Figure 1 and CD38 activity studies were obtained from the NIA (National Institute on Aging). In all head-to-head comparisons of WT, CD38KO, or CD38/SIRT3KO, in-house-generated litter mates were used.

Western Blot

Mouse tissues and cultured cells were lysed in NETN (20 mM Tris-HCl (pH 8.0), 100 mM NaCl, 1 mM EDTA, and 0.5% NP-40) buffer supplemented with 5 mM NaF, 50 mM 2-glycerophosphate, and a protease inhibitor cocktail (Roche). Western blots were developed using horseradish peroxidase-conjugated secondary antibodies or protein A-HRP and SuperSignal West Pico chemiluminescent substrate (Pierce). The anti-human CD38 antibody was from Abcam. Anti-mouse primary antibodies were as follows: CD38 from Santa Cruz; acetylated lysine, PARP1, SIRT1, and SIRT3 from Cell Signaling; COX IV and tubulin from Abcam; PBEF/NAMPT from Bethyl Laboratories, and actin from Sigma. The anti-mouse PAR antibody was a kind gift from Dr. Scott Kaufmann.

Mitochondrial Function

Mitochondria were isolated by differential centrifugation at 4°C followed by percoll (Invitrogen) gradient. Deacetylase inhibitors, trichostatin A (TSA) (5 μM) and nicotinamide (5 mM), were added to isolation buffer. The final LM pellet was re-suspended in MIR05 + fatty acid-free BSA (1 mg/mL) at a final protein concentration of 10–15 mg/mL for respiration experiments or frozen for other experiments (see Supplemental Information for more details). The O_2 consumption rates were measured polarographically using high-resolution respirometry (Oroboros Oxygraph-O2K) and Data Lab software (Gnaiger, 2009). Membrane potential was measured using the fluorescence signal of the cationic dye, safranin-O. Tissue mitochondrial content was measured by quantitative real-time PCR and expressed as a ratio of mtDNA to genomic DNA (see Supplemental Information for details).

Determination of NAD^+, NADH, and NAD^+ Precursors

Detection of NAD^+ and NADH was performed as described before using the cycling assay (Aksoy et al., 2006) and a UPLC-mass spectroscopy assay (Supplemental Experimental Procedures). The specificity of the cycling assay for NAD^+ and NADH was determined as shown in Figure S1. Briefly, samples were extracted with 10% TCA at 4°C. TCA was removed with water-saturated ether. NADH was extracted with 500 mM NaOH and 5 mM EDTA and heated for 30 min at 60°C. The aqueous layer containing the nucleotides was removed and adjusted to pH 8 with 1 M Tris. Fractions were stored at −80°C. In control experiments, we have used known concentration of NAD^+ and NADH and exposed them to the same extraction protocols used in our studies. We observed that nearly 95% of NAD^+ and undetectable levels of NADH remained after the acid extraction with TCA. Furthermore, the reverse was true for NaOH extraction, where most of the NAD^+ was lost and nearly 95% of the NADH was preserved. We have also measured CD38 NADase activity after the TCA and NaOH treatment and found that both treatments completely destroyed the CD38 NADase activity.

Nicotinamide was measured by a coupled assay containing nicotinamidase (PNC1) (Smith et al., 2009). NR, NMN, NAM, and NAD^+ in blood samples were detected using an HPLC system (Shimadzu) based on Yoshino and Imai (2013); details are in Supplemental Information.

Enzyme Activity

CD38 activity was measured according to Aksoy et al. (2006). In vitro CD38 activity was measured using 0.1 U of recombinant human CD38 (R&D Systems) in 0.25 M sucrose and 40 mM Tris-HCl (pH 7.4). Nicotinamide 1, N6-ethenoadenine di-nucleotide was used to determine NADase activity. Lactate released in media was measured by the lactate dehydrogenase coupled assay (Hamilton and Pardue, 1984). Citrate synthase was measured as described (Kuznetsov et al., 2008). Briefly, cell extract was incubated with a buffer containing 100 mM Tris (pH 8.0), 0.1 mM acetyl-CoA, 0.1 mM 5,5′-dithiobis-(2-nitrobenzoic acid), and 0.1% Triton X-100. The assay started with the addition of 0.2 mM oxaloacetate and was monitored at 412 nm for 10 min at 25°C. SIRT3 activity was determined by a fluorometric method using SIRT3 Direct Fluorescence Screening Assay Kit (Cayman). Protein concentration was determined using Bio-Rad Protein Reagent.

Statistical Analysis

Data were analyzed by a two-tailed Student's t test and ANOVA. Statistical analysis was performed using GraphPad Prism 6.

SUPPLEMENTAL INFORMATION

Supplemental Information includes Supplemental Experimental Procedures, six figures, and two tables and can be found with this article online at http://dx.doi.org/10.1016/j.cmet.2016.05.006.

AUTHOR CONTRIBUTIONS

E.N.C., J.C.-P., and C.C.S.C. generated the hypothesis and concept of the manuscript; E.N.C. and J.C.-P. were involved in conduction and designed all experiments. J.C.-P., M.G.T., and G.M.W. performed the mitochondrial studies; E.N.C., J.C.-P., and A.G. analyzed and interpreted the mitochondrial data; and J.C.-P., M.G.T., and C.C.S.C. performed cell experiments, western blots, and PCRs. A.S.P. performed flow cytometry, and J.C.-P., M.G.T., C.E., V.N., R.A.S., J.M.R., and E.N.C. designed, performed, and interpreted nucleotide measurement experiments. J.C.-P., M.G.T., C.E., and V.N. performed animal studies. All authors contributed to writing the manuscript.

ACKNOWLEDGMENTS

This work was supported in part by grants from the American Federation for Aging Research, the Mayo Foundation, the Strickland Career Development Award, NIH grants from the National Institute of Aging (NIA, grant AG-26094) and the National Institute of Diabetes and Digestive and Kidney Diseases (NIDDK, grant DK-084055), Mayo-UOFM Decade of Discovery Grant 63-01, and Minnesota Obesity Council Grant DK-50456-15. J.C.-P. is supported by grants from the Conselho Nacional de Desenvolvimento Científico e Tecnológico/Brazil(CNPQ) and Fundação de Amparo é Pesquisa do Rio de Janeiro/Brazil (FAPERJ). E.N.C. holds patents on the use of CD38 inhibitors.

Received: April 27, 2015
Revised: February 8, 2016
Accepted: May 22, 2016
Published: June 14, 2016

REFERENCES

Aksoy, P., White, T.A., Thompson, M., and Chini, E.N. (2006). Regulation of intracellular levels of NAD: a novel role for CD38. Biochem. Biophys. Res. Commun. *345*, 1386–1392.

Bai, P., and Cantó, C. (2012). The role of PARP-1 and PARP-2 enzymes in metabolic regulation and disease. Cell Metab. *16*, 290–295.

Bai, P., Cantó, C., Oudart, H., Brunyánszki, A., Cen, Y., Thomas, C., Yamamoto, H., Huber, A., Kiss, B., Houtkooper, R.H., et al. (2011). PARP-1 inhibition increases mitochondrial metabolism through SIRT1 activation. Cell Metab. *13*, 461–468.

Bakondi, E., Catalgol, B., Bak, I., Jung, T., Bozaykut, P., Bayramicli, M., Ozer, N.K., and Grune, T. (2011). Age-related loss of stress-induced nuclear

proteasome activation is due to low PARP-1 activity. Free Radic. Biol. Med. *50*, 86–92.

Barata, H., Thompson, M., Zielinska, W., Han, Y.S., Mantilla, C.B., Prakash, Y.S., Feitoza, S., Sieck, G., and Chini, E.N. (2004). The role of cyclic-ADP-ribose-signaling pathway in oxytocin-induced Ca2+ transients in human myometrium cells. Endocrinology *145*, 881–889.

Barbosa, M.T.P., Soares, S.M., Novak, C.M., Sinclair, D., Levine, J.A., Aksoy, P., and Chini, E.N. (2007). The enzyme CD38 (a NAD glycohydrolase, EC 3.2.2.5) is necessary for the development of diet-induced obesity. FASEB J. *21*, 3629–3639.

Beneke, S., Scherr, A.-L., Ponath, V., Popp, O., and Bürkle, A. (2010). Enzyme characteristics of recombinant poly(ADP-ribose) polymerases-1 of rat and human origin mirror the correlation between cellular poly(ADP-ribosyl)ation capacity and species-specific life span. Mech. Ageing Dev. *131*, 366–369.

Bieganowski, P., and Brenner, C. (2004). Discoveries of nicotinamide riboside as a nutrient and conserved NRK genes establish a Preiss-Handler independent route to NAD+ in fungi and humans. Cell *117*, 495–502.

Blacher, E., Dadali, T., Bespalko, A., Haupenthal, V.J., Grimm, M.O., Hartmann, T., Lund, F.E., Stein, R., and Levy, A. (2015). Alzheimer's disease pathology is attenuated in a CD38-deficient mouse model. Ann. Neurol. *78*, 88–103.

Braidy, N., Guillemin, G.J., Mansour, H., Chan-Ling, T., Poljak, A., and Grant, R. (2011). Age related changes in NAD+ metabolism oxidative stress and Sirt1 activity in wistar rats. PLoS ONE *6*, e19194.

Cantó, C., Houtkooper, R.H., Pirinen, E., Youn, D.Y., Oosterveer, M.H., Cen, Y., Fernandez-Marcos, P.J., Yamamoto, H., Andreux, P.A., Cettour-Rose, P., et al. (2012). The NAD(+) precursor nicotinamide riboside enhances oxidative metabolism and protects against high-fat diet-induced obesity. Cell Metab. *15*, 838–847.

Chini, E.N. (2009). CD38 as a regulator of cellular NAD: a novel potential pharmacological target for metabolic conditions. Curr. Pharm. Des. *15*, 57–63.

Chini, C.C., Guerrico, A.M., Nin, V., Camacho-Pereira, J., Escande, C., Barbosa, M.T., and Chini, E.N. (2014). Targeting of NAD metabolism in pancreatic cancer cells: potential novel therapy for pancreatic tumors. Clin. Cancer Res. *20*, 120–130.

Di Lisa, F., Menabò, R., Canton, M., Barile, M., and Bernardi, P. (2001). Opening of the mitochondrial permeability transition pore causes depletion of mitochondrial and cytosolic NAD+ and is a causative event in the death of myocytes in postischemic reperfusion of the heart. J. Biol. Chem. *276*, 2571–2575.

Escande, C., Nin, V., Price, N.L., Capellini, V., Gomes, A.P., Barbosa, M.T., O'Neil, L., White, T.A., Sinclair, D.A., and Chini, E.N. (2013). Flavonoid apigenin is an inhibitor of the NAD+ ase CD38: implications for cellular NAD+ metabolism, protein acetylation, and treatment of metabolic syndrome. Diabetes *62*, 1084–1093.

Finley, L.W., Haas, W., Desquiret-Dumas, V., Wallace, D.C., Procaccio, V., Gygi, S.P., and Haigis, M.C. (2011). Succinate dehydrogenase is a direct target of sirtuin 3 deacetylase activity. PLoS ONE *6*, e23295.

Frasca, L., Fedele, G., Deaglio, S., Capuano, C., Palazzo, R., Vaisitti, T., Malavasi, F., and Ausiello, C.M. (2006). CD38 orchestrates migration, survival, and Th1 immune response of human mature dendritic cells. Blood *107*, 2392–2399.

Ghosh, S., Lertwattanarak, R., Garduño, Jde.J., Galeana, J.J., Li, J., Zamarripa, F., Lancaster, J.L., Mohan, S., Hussey, S., and Musi, N. (2015). Elevated muscle TLR4 expression and metabolic endotoxemia in human aging. J. Gerontol. A Biol. Sci. Med. Sci. *70*, 232–246.

Gnaiger, E. (2009). Capacity of oxidative phosphorylation in human skeletal muscle: new perspectives of mitochondrial physiology. Int. J. Biochem. Cell Biol. *41*, 1837–1845.

Gomes, A.P., Price, N.L., Ling, A.J.Y., Moslehi, J.J., Montgomery, M.K., Rajman, L., White, J.P., Teodoro, J.S., Wrann, C.D., Hubbard, B.P., et al. (2013). Declining NAD(+) induces a pseudohypoxic state disrupting nuclear-mitochondrial communication during aging. Cell *155*, 1624–1638.

Grozio, A., Sociali, G., Sturla, L., Caffa, I., Soncini, D., Salis, A., Raffaelli, N., De Flora, A., Nencioni, A., and Bruzzone, S. (2013). CD73 protein as a source of extracellular precursors for sustained NAD+ biosynthesis in FK866-treated tumor cells. J. Biol. Chem. *288*, 25938–25949.

Guedes, A.G., Jude, J.A., Paulin, J., Kita, H., Lund, F.E., and Kannan, M.S. (2008). Role of CD38 in TNF-α-induced airway hyperresponsiveness. Am. J. Physiol. Lung Cell. Mol. Physiol. *294*, L290–L299.

Haffner, C.D., Becherer, J.D., Boros, E.E., Cadilla, R., Carpenter, T., Cowan, D., Deaton, D.N., Guo, Y., Harrington, W., Henke, B.R., et al. (2015). Discovery, synthesis, and biological evaluation of thiazoloquin(az)olin(on)es as potent CD38 inhibitors. J. Med. Chem. *58*, 3548–3571.

Hamilton, S.D., and Pardue, H.L. (1984). Quantitation of lactate by a kinetic method with an extended range of linearity and low dependence on experimental variables. Clin. Chem. *30*, 226–229.

Hirschey, M.D., Shimazu, T., Goetzman, E., Jing, E., Schwer, B., Lombard, D.B., Grueter, C.A., Harris, C., Biddinger, S., Ilkayeva, O.R., et al. (2010). SIRT3 regulates mitochondrial fatty-acid oxidation by reversible enzyme deacetylation. Nature *464*, 121–125.

Imai, S., and Guarente, L. (2014). NAD+ and sirtuins in aging and disease. Trends Cell Biol. *24*, 464–471.

Kim, K.A., Jeong, J.J., Yoo, S.Y., and Kim, D.H. (2016). Gut microbiota lipopolysaccharide accelerates inflamm-aging in mice. BMC Microbiol. *16*, 9.

Kirkwood, T.B., and Rose, M.R. (1991). Evolution of senescence: late survival sacrificed for reproduction. Philos. Trans. R. Soc. Lond. B Biol. Sci. *332*, 15–24.

Kuznetsov, A.V., Veksler, V., Gellerich, F.N., Saks, V., Margreiter, R., and Kunz, W.S. (2008). Analysis of mitochondrial function in situ in permeabilized muscle fibers, tissues and cells. Nat. Protoc. *3*, 965–976.

Lanza, I.R., and Nair, K.S. (2010). Mitochondrial function as a determinant of life span. Pflugers Arch. *459*, 277–289.

Lee, C.U., Song, E.K., Yoo, C.H., Kwak, Y.K., and Han, M.K. (2012). Lipopolysaccharide induces CD38 expression and solubilization in J774 macrophage cells. Mol. Cells *34*, 573–576.

Malavasi, F., Deaglio, S., Funaro, A., Ferrero, E., Horenstein, A.L., Ortolan, E., Vaisitti, T., and Aydin, S. (2008). Evolution and function of the ADP ribosyl cyclase/CD38 gene family in physiology and pathology. Physiol. Rev. *88*, 841–886.

Massudi, H., Grant, R., Braidy, N., Guest, J., Farnsworth, B., and Guillemin, G.J. (2012). Age-associated changes in oxidative stress and NAD+ metabolism in human tissue. PLoS ONE *7*, e42357.

Nahimana, A., Attinger, A., Aubry, D., Greaney, P., Ireson, C., Thougaard, A.V., Tjørnelund, J., Dawson, K.M., Dupuis, M., and Duchosal, M.A. (2009). The NAD biosynthesis inhibitor APO866 has potent antitumor activity against hematologic malignancies. Blood *113*, 3276–3286.

Noren Hooten, N., Fitzpatrick, M., Kompaniez, K., Jacob, K.D., Moore, B.R., Nagle, J., Barnes, J., Lohani, A., and Evans, M.K. (2012). Coordination of DNA repair by NEIL1 and PARP-1: a possible link to aging. Aging (Albany, N.Y.) *4*, 674–685.

Polzonetti, V., Carpi, F.M., Micozzi, D., Pucciarelli, S., Vincenzetti, S., and Napolioni, V. (2012). Population variability in CD38 activity: correlation with age and significant effect of TNF-α -308G>A and CD38 184C>G SNPs. Mol. Genet. Metab. *105*, 502–507.

Prolla, T.A., and Denu, J.M. (2014). NAD+ deficiency in age-related mitochondrial dysfunction. Cell Metab. *19*, 178–180.

Scheibye-Knudsen, M., Mitchell, S.J., Fang, E.F., Iyama, T., Ward, T., Wang, J., Dunn, C.A., Singh, N., Veith, S., Hasan-Olive, M.M., et al. (2014). A high-fat diet and NAD(+) activate Sirt1 to rescue premature aging in cockayne syndrome. Cell Metab. *20*, 840–855.

Shimazu, T., Hirschey, M.D., Hua, L., Dittenhafer-Reed, K.E., Schwer, B., Lombard, D.B., Li, Y., Bunkenborg, J., Alt, F.W., Denu, J.M., et al. (2010). SIRT3 deacetylates mitochondrial 3-hydroxy-3-methylglutaryl CoA synthase 2 and regulates ketone body production. Cell Metab. *12*, 654–661.

Smith, B.C., Hallows, W.C., and Denu, J.M. (2009). A continuous microplate assay for sirtuins and nicotinamide-producing enzymes. Anal. Biochem. *394*, 101–109.

Sun, L., Adebanjo, O.A., Koval, A., Anandatheerthavarada, H.K., Iqbal, J., Wu, X.Y., Moonga, B.S., Wu, X.B., Biswas, G., Bevis, P.J., et al. (2002). A novel mechanism for coupling cellular intermediary metabolism to cytosolic Ca2+ signaling via CD38/ADP-ribosyl cyclase, a putative intracellular NAD+ sensor. FASEB J. *16*, 302–314.

Tao, R., Coleman, M.C., Pennington, J.D., Ozden, O., Park, S.H., Jiang, H., Kim, H.S., Flynn, C.R., Hill, S., Hayes McDonald, W., et al. (2010). Sirt3-mediated deacetylation of evolutionarily conserved lysine 122 regulates MnSOD activity in response to stress. Mol. Cell *40*, 893–904.

Yamada, M., Mizuguchi, M., Otsuka, N., Ikeda, K., and Takahashi, H. (1997). Ultrastructural localization of CD38 immunoreactivity in rat brain. Brain Res. *756*, 52–60.

Yang, H., Yang, T., Baur, J.A., Perez, E., Matsui, T., Carmona, J.J., Lamming, D.W., Souza-Pinto, N.C., Bohr, V.A., Rosenzweig, A., et al. (2007). Nutrient-sensitive mitochondrial NAD+ levels dictate cell survival. Cell *130*, 1095–1107.

Yoshino, J., and Imai, S. (2013). Accurate measurement of nicotinamide adenine dinucleotide (NAD^+) with high-performance liquid chromatography. Methods Mol. Biol. *1077*, 203–215.

Yoshino, J., Mills, K.F., Yoon, M.J., and Imai, S. (2011). Nicotinamide mononucleotide, a key NAD(+) intermediate, treats the pathophysiology of diet- and age-induced diabetes in mice. Cell Metab. *14*, 528–536.

Yu, W., Dittenhafer-Reed, K.E., and Denu, J.M. (2012). SIRT3 protein deacetylates isocitrate dehydrogenase 2 (IDH2) and regulates mitochondrial redox status. J. Biol. Chem. *287*, 14078–14086.

Zhang, H., Xiong, Z.-M., and Cao, K. (2014). Mechanisms controlling the smooth muscle cell death in progeria via down-regulation of poly(ADP-ribose) polymerase 1. Proc. Natl. Acad. Sci. USA *111*, E2261–E2270.

Zhu, X.H., Lu, M., Lee, B.Y., Ugurbil, K., and Chen, W. (2015). In vivo NAD assay reveals the intracellular NAD contents and redox state in healthy human brain and their age dependences. Proc. Natl. Acad. Sci. USA *112*, 2876–2881.

Cell Metabolism, Volume *23*

Supplemental Information

CD38 Dictates Age-Related NAD Decline and Mitochondrial Dysfunction through an SIRT3-Dependent Mechanism

Juliana Camacho-Pereira, Mariana G. Tarragó, Claudia C.S. Chini, Veronica Nin, Carlos Escande, Gina M. Warner, Amrutesh S. Puranik, Renee A. Schoon, Joel M. Reid, Antonio Galina, and Eduardo N. Chini

TABLE S1, related to Figure 3. Mitochondrial Respiration Rates with Different Substrates

Liver Mitochondria	***Wild-Type***	***CD38KO***
Glutamate		
State II	28.3 ± 9.4	53.6 ± 12.1*
State III	121.6 ± 19	209 ± 18*
State IV	38.3 ± 9.8	60 ± 16*
Uncoupled	127.3 ± 25	202 ± 4.2*
Palmytoil-Carnitine +Malate		
State II	54.5 ± 13	77 ± 28*
State III	91.5 ± 21	121 ± 24*
State IV	42.5 ± 10	53 ± 98*
Uncoupled	102 ± 15	140 ± 18

TABLE S2, related to Figure 3. Spleen Mitochondrial Respiration Rates

Spleen Mitochondria	***Wild-Type***	***CD38KO***
Succinate+Rotenone		
State II	127 ± 2.8	304 ± 105*
State III	223 ± 47	456 ± 145
State IV	54 ± 6.3	104 ± 12*
Uncoupled	197 ± 71	534± 194*

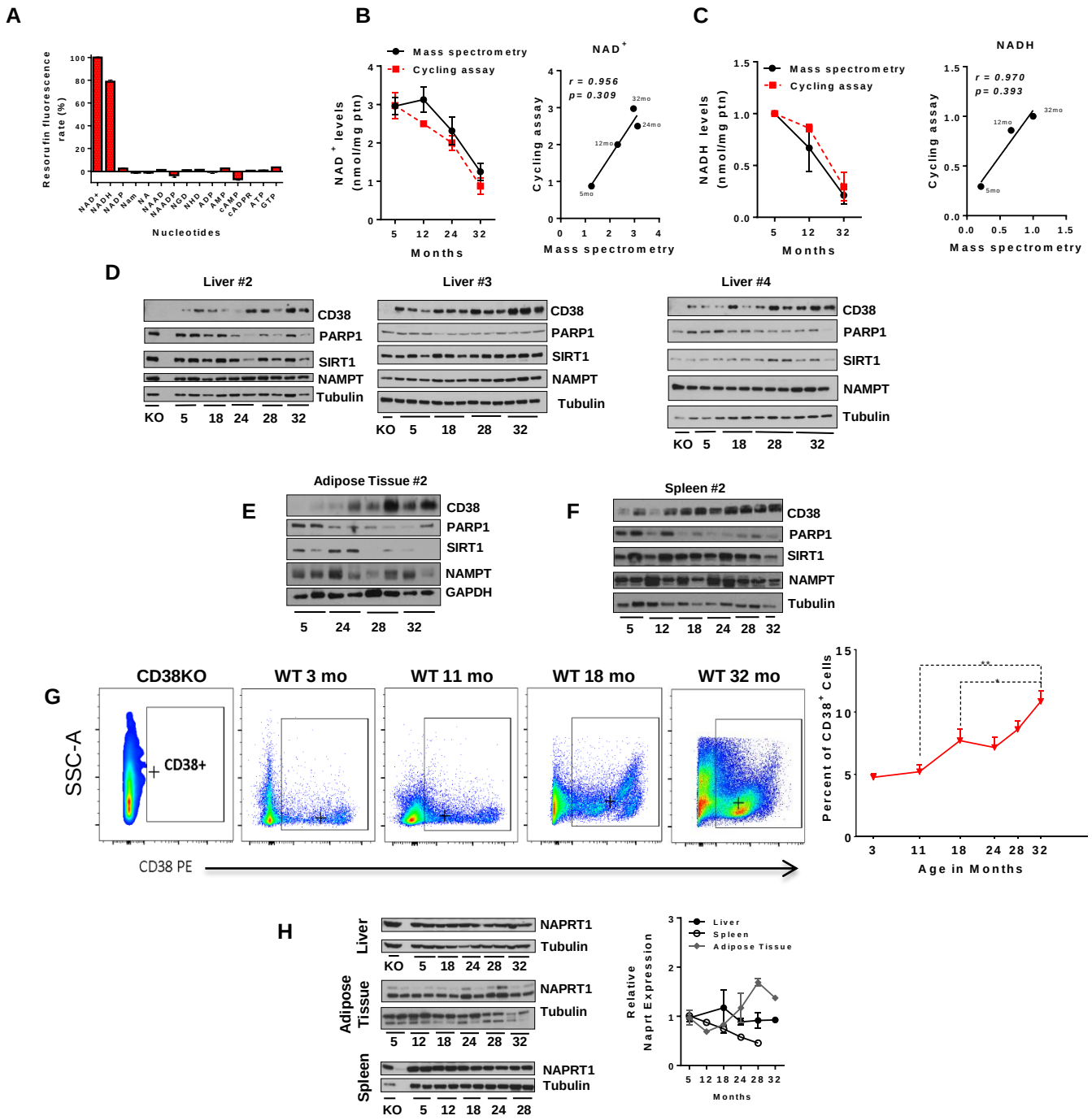

Figure S1, related to Figure 1. **(A)** Resorufin fluorescence rate using the alcohol dehydrogenase reaction. Experimental conditions were the same for all nucleotides (50nM). Results are means ± S.E from three independent measurements, normalized against NAD+ levels. **(B)** Total NAD^+ levels in WT and CD38KO mice liver tissue during aging measured by two methods: mass spectroscopy (black line) and cycling assay (red dotted line), (n=4). The Pearson correlation coefficient (r) was: r = 0.956. **(C)** NADH levels in WT and CD38KO mice liver tissue during aging measured by two methods: mass spectroscopy (black line) and cycling assay (red dotted line), (n=4). The Pearson correlation coefficient (r) was: r = 0.970. **(D-F)** Immunoblots for CD38, NAMPT, PARP1, and SIRT1 in liver **(D)**, adipose tissue **(E)** and spleen **(F)** of mice in different ages. **(G)** Flow cytometric assessment of CD38+ cells in mouse liver with aging. Representative flow plots showing analysis of CD38+ population in liver of CD38KO (negative control) and C57BL6 mice at 3, 11, 18, and 32 months of age; graph shows mean ± SEM for n=4 mice per age (*p<0.05, **p<0.01 versus 11 mo. old). **(H)** Immunoblots for NAPRT1 in liver, adipose tissue and spleen of mice in different ages. On the right, graph shows mean + SEM of relative protein expression of NAPRT1. Relative expression of the protein was calculated to Tubulin in each lane and then calculated relative to 5 month old mice (*p<0.05).

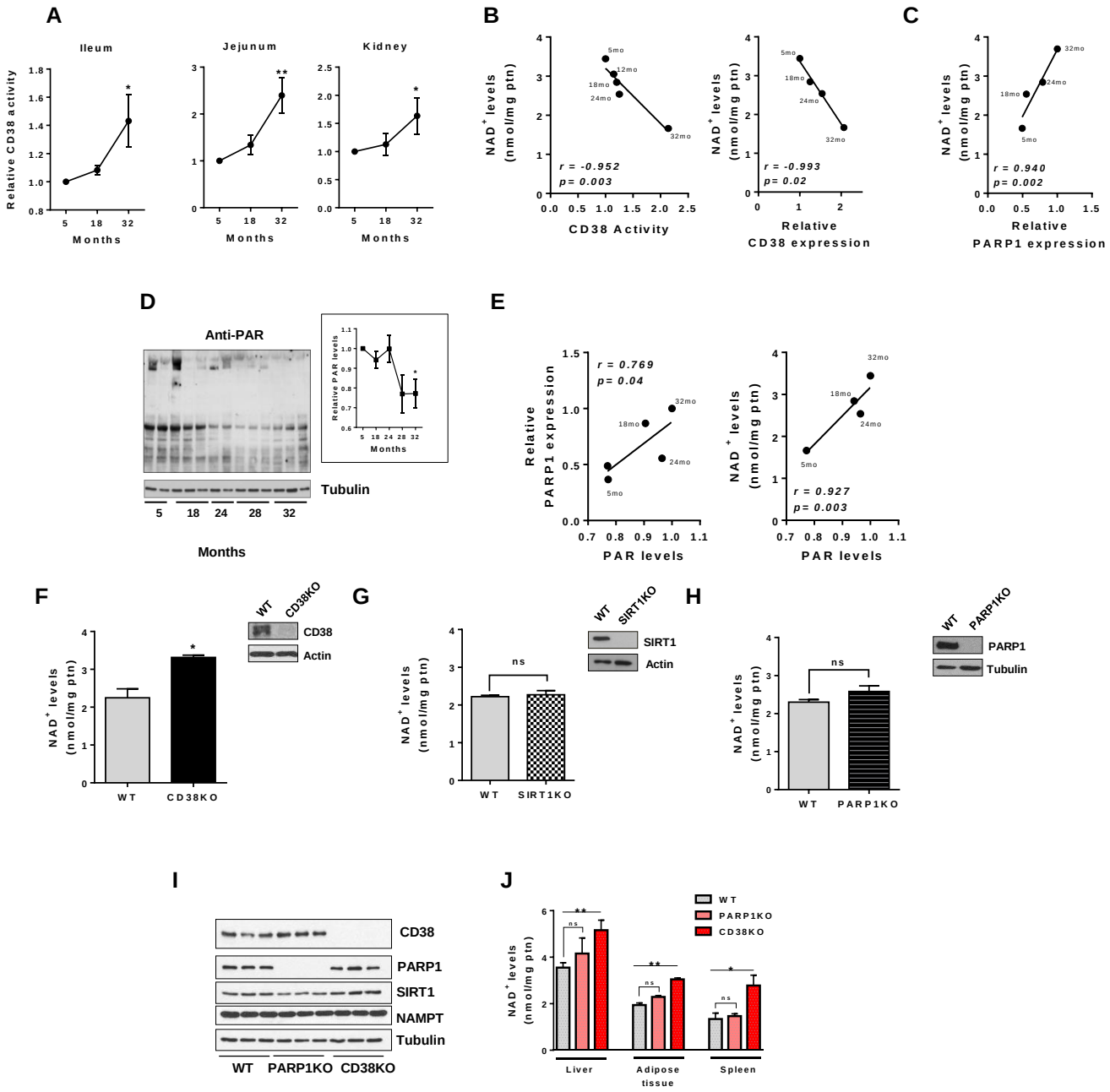

Figure S2, related to Figure 2 . **(A)** CD38 activity in ileum, jejunum and kidney of mice of different ages (n=4, *p<0.05 versus 5 month old mice). **(B)** NAD^+ levels of aging mice liver tissue are plotted against relative CD38 activity or CD38 protein expression. The Pearson correlation coefficient (r) was significant in both cases: r = −0.95, p= 0.003 and r=-0.99, p= 0.02, respectively. **(C)** Pearson correlation coefficient (r) and corresponding p-value between NAD^+ levels of aging mice liver tissue and the relative PARP1 protein expression is displayed. **(D)** Immunoblots for PAR and Tubulin in mice liver tissue (left). On the right, graph shows relative protein expression of PAR, calculated as a ratio to Tubulin in each lane, and then calculated relative to 5 month old mice (n=3, *p<0.05). **(E)** PAR levels of aging mice liver tissue are plotted against relative PARP1 protein expression and NAD^+ levels. The Pearson correlation coefficient (r) was significant in both cases: r = 0.769, p= 0.04 and r= 0.927, p= 0.003, respectively. **(F-H)** NAD+ levels in primary mouse embryonic fibroblasts (MEFs) purified and cultured from wild-type (WT), CD38 knockout (F), SIRT1 knockout (G), and PARP1 knockout (H) mice (n=5, **p<0.001, ns=non-significant (p>0.05) versus WT). **(I)** Immunoblots for CD38, NAMPT, PARP1, SIRT1 and Tubulin in liver of WT, PARP1KO and CD38KO mice, each lane shows one independent mouse. **(J)** NAD^+ levels in liver, adipose tissue and spleen of WT, PARP1KO and CD38KO mice (n=4, *p<0.05, **p<0.001, ns=non-significant (p>0.05).

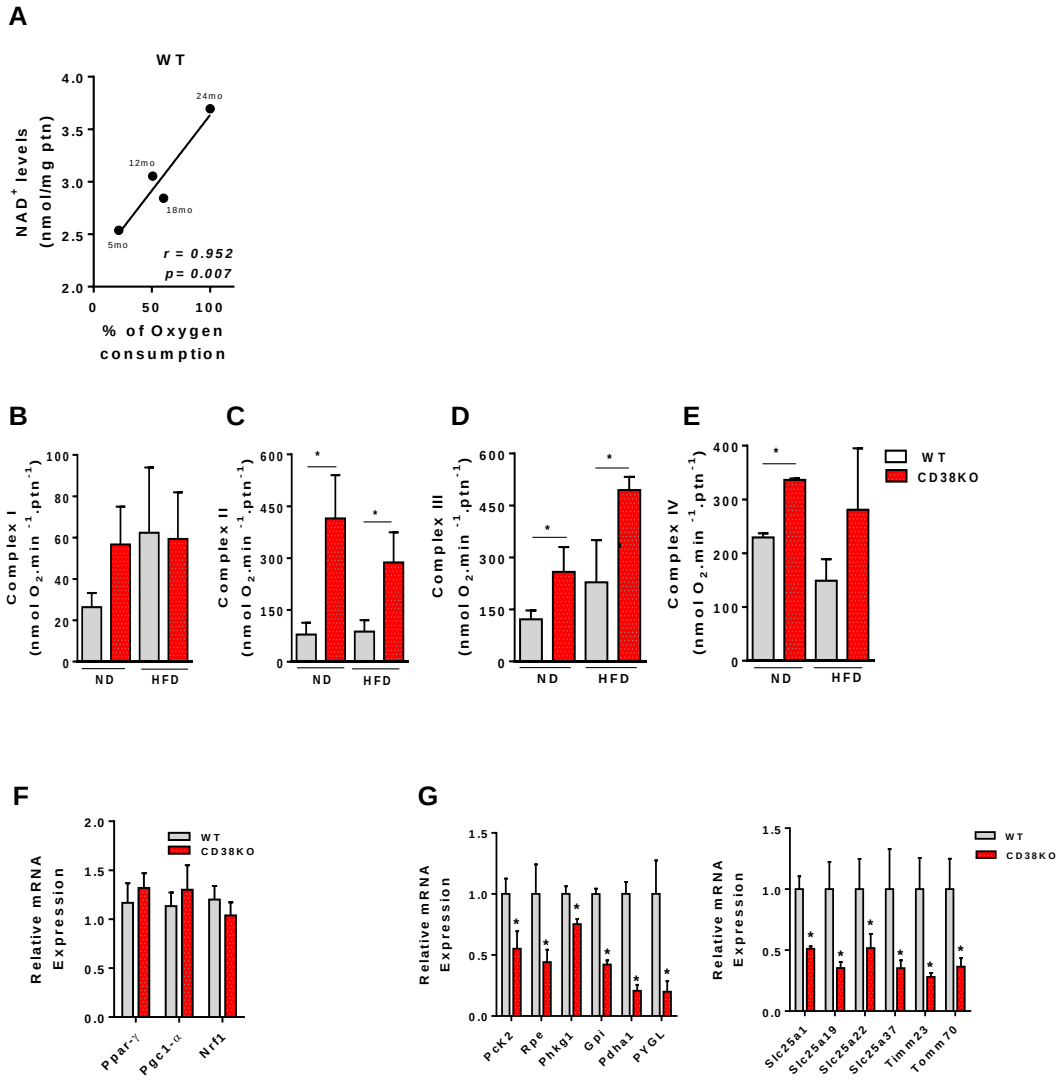

Figure S3, related to Figure 3. (A) Correlation between age-related decrease in NAD^+ levels and mitochondrial function. NAD+ levels of aging WT mice liver tissue are plotted against the percentage of oxygen consumption. The Pearson correlation coefficient (r) is significant: r = 0.952, p= 0.007. **(B-E)** Mitochondrial complex I (NADH:Ubiquinol oxireductase) activity **(B)**, complex II activity **(C)**, complex III activity **(D)** and complex VI activity **(E)** measured in intact mitochondria isolated from two year old litter mate WT and CD38 KO mice submitted to 16 weeks of normal (ND) or high fat diet, 42% of fat (HFD). (n=5, * p <0.05 versus WT mice, normal diet). **(F)** Relative mRNA expression of genes related to mitochondria biogenesis in liver from one year old WT and CD38KO mice. (n=4, * p <0.05 versus WT mice). **(G)** Relative mRNA expression in liver from one year old CD38KO mice compared to WT. The genes encoded the related proteins: *Pck2* (mitochondrial phosphoenolpyruvate carboxykinase (GTP) family), *Rpe* (ribulose-5-phosphate-epimerase), *PhgK1* (pyruvate kinase subunit – glycogenolytic regulatory enzyme), *Gpi* (phosphoglucose isomerase), *Pdha1* (pyruvate dehydrogenase subunit E1 alpha1), *Pygl* (liver glycogen phosphorylase), *Slc25a1* (mitochondrial citrate transport protein, CTP), *Slc25a19* (mitochondrial thiamine pyrophosphate carrier), *Slc25a22* (mitochondrial glutamate carrier), *Slc25a37* (mitochondrial iron transporter), *Timm23* (mitochondrial import inner membrane translocase subunit), *Tomm70* (translocase of outer mitochondrial membrane 70 homolog A (S. cerevisiae)). (n=4, *p<0.05 versus WT mice)

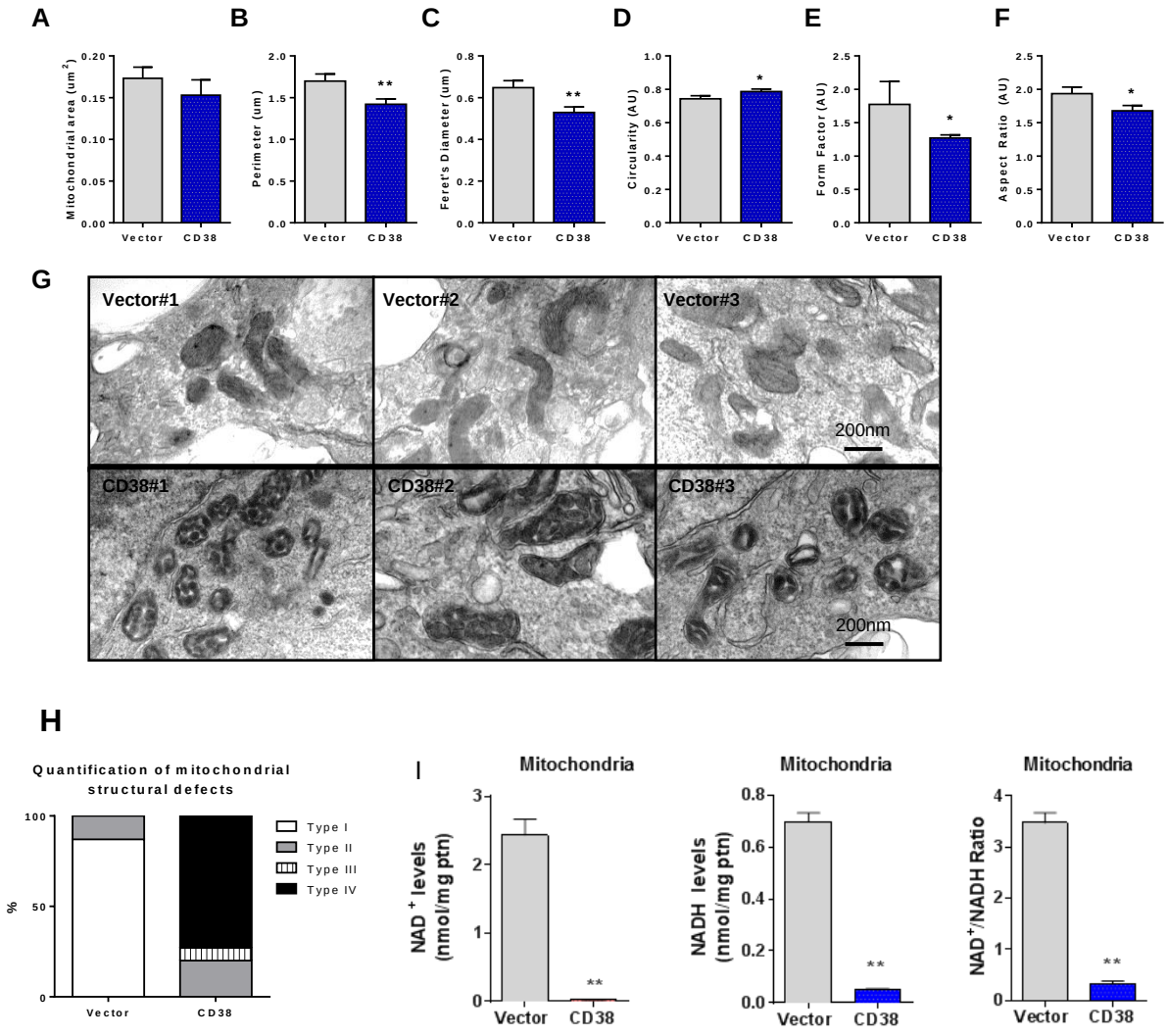

Figure S4, related to Figure 4. **Effects of CD38 overexpression in mitochondrial morphology. (A-F)** Mitochondrial size parameters: area **(A)**, perimeter **(B)**, and Feret's diameter **(C)**. Mitochondrial shape descriptors : circularity **(D),** form factor **(E)** and aspect ratio **(F)**. (A-F) n =48 control mitochondria and n=64 CD38 mitochondria from 3 different experiments. Mean ± SEM. (*AU* arbitrary units); $*p < 0.05$, $**p < 0.01$. **(G)** Transmission Electron Microscopy (TEM) in cells transfected with empty vector (upper panel) or CD38 (lower panel). The scale bar is 200 nm for all three independent experiments in each group shown in the figure. **(H)** Quantification of mitochondrial ultrastructural defects. Blinded subjects were asked to score TEM images based on a score described in the methods section. Percentages of TEM images with intact mitochondria with normal appearing cristae (Type I); abnormal mitochondria with either swollen, irregular or whorling cristae (Type II); mitochondria with discontinuous outer membrane or deficient cristae (Type III); and mitochondria with both swollen and deficient cristae or both discontinues outer membrane and swollen cristae (Type IV) have been expressed from a total pool of 8 independent TEM pictures of each group presented to the subjects. **(I)** Mitochondria were isolated from cells transfected with empty vector (gray) or CD38 (blue). After isolation content of nucleotides were measured by cycling assay n=4, $**p < 0.01$.

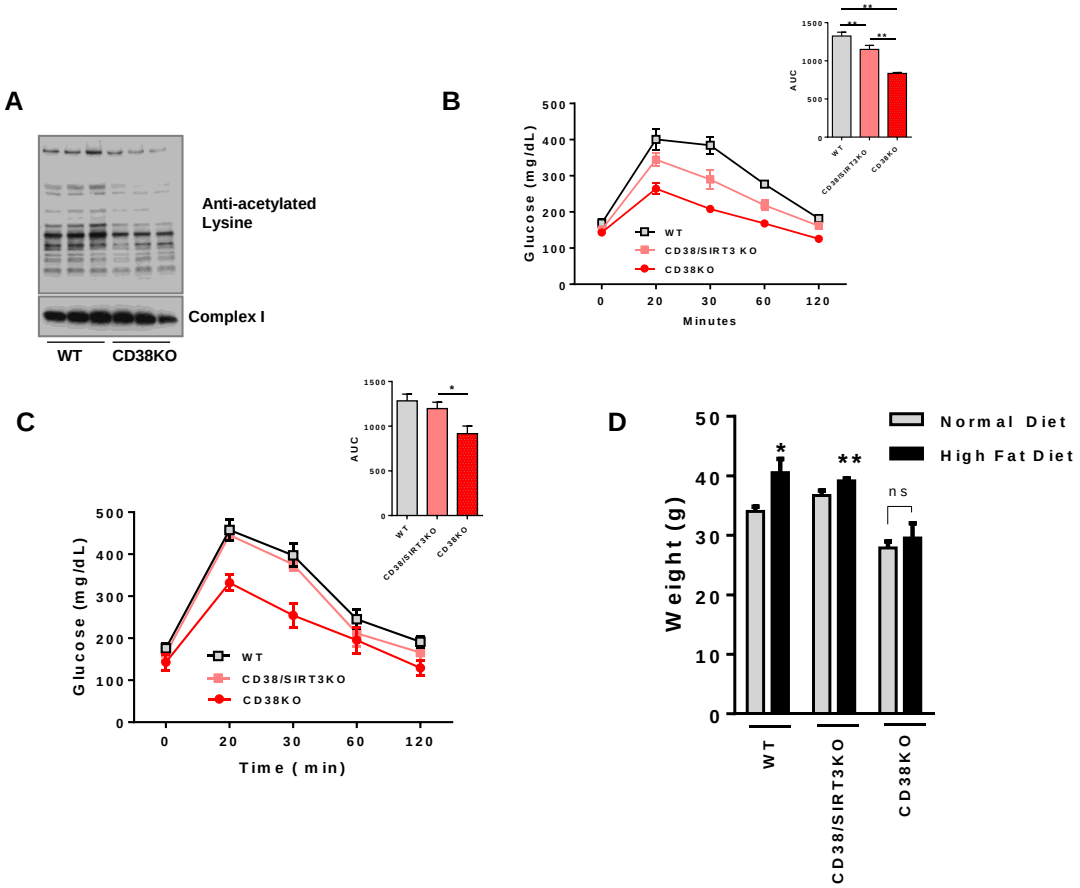

Figure S5, related to Figure 5. (A) Mitochondrial protein acetylation profile from six different mice than in figure 5 mice were one year old. **(B)** Glucose concentration in one year old WT, CD38/SIRT3KO and CD38KO mice in normal chow. Inset: Area under the curve from experiments (n=10, * p <0.05 versus WT mice). **(C)** Glucose concentration in one year old WT, CD38/SIRT3KO and CD38KO mice after 16 weeks of high fat diet. Inset: Area under the curve from experiments (n=10, * p <0.05 versus WT mice). **(D)** Body weight of one year old mice on normal chow diet and after 16 weeks of high fat diet (n=10, * p <0.05 versus mice in normal diet). The mice in B-C were one year old at the beginning of the study.

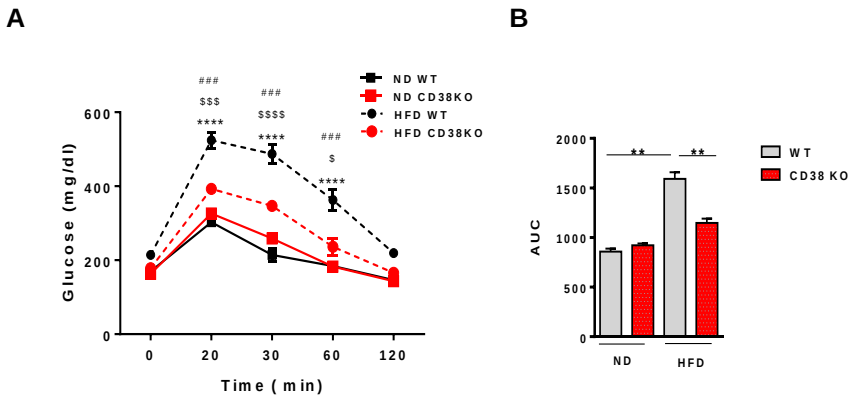

Figure S6, related to Figure 6. (A) Glucose concentration in 24 month old WT and CD38KO mice after intraperitoneal injection of glucose. Experiments made before and after 16 weeks of high fat diet. Area under the curve for glucose concentrations in different mice (**p<0.01, n=10). Data are expressed as means±SE. **(B)**. Two-way ANOVA and Bonferroni's post-test with repeated measures show significant interaction between the glucose curve for HFD WT and HFD CD38KO (****p<0.001*); ND CD38KO and HFD CD38KO (*$ p<0.05, $$$ p<0.001, $$$$ p<0.0001*); and ND WT and HFD WT (*### p<0.001*).

SUPPLEMENTAL EXPERIMENTAL PROCEDURES

Animal Studies

CD38/SIRT3 double KO mice (Figure 5) were generated by crossing CD38KO mice (C57BL/6 background) with SIRT3KO mice (129S background) to produce double heterozygous mice. These mice were then crossed, and the offspring genotyped for CD38 and SIRT3 mutations by PCR. CD38 primers were: oIMR0092 (*5'-AAT CCA TCT TGT TCA ATG GCC GAT C-3'*), oIMR7727 (*5'-CAC CAT AAG AGG GGA AGC AA-3'*), and oIMR7728 (*5'-TGC CAA AAG TGC AGA AGA GA-3'*). SIRT-3 primers were: SIRT3-KO -1*(5'-CTT CTG CGC CTC TAT ACA CAG-3'),* SIRT3-KO-2 *(5-TGC AAC AAG GCT TTA TCT TCC-3')* and SIRT3-KO-3*(5'-TAC TGA ATA TCA GTG GGA ACG-3').* PCR products were separated by agarose gel electrophoresis and visualized by ethidium bromide staining. After three crosses of the heterozygous the F3 generation was used for the generation of the animals used for the our experiments. CD38KO animals that were wild type or knockout for SIRT3 were used for experiments. Importantly, all mice used in the double knockout studies (non-mutant, CD38 single mutant and CD38/SIRT3 double mutant) were on a mixed C57BL6/129S background (the mixed background was present only on the animals used for the experiments of figure 5. All other wild type and CD38 KO mice were on a pure C57BL6 background. The experiments presented in figure 1 were performed with wild type animals from the aging NIA animal colony (CD38 KO tissues were used in these experiments to demonstrate the specificity of the CD38 antibody used). The same results as presented in figure 1, namely increase in CD38 expression with aging, were also observed when we assayed the same parameters in our own wild type mice that were generated by heterozygous cross of our CD38 colony. Except for figure 1 and figure 5, in all other animal experiments the comparison is made between wild type and CD38 KO litter mates in a pure C57BL6 background. Mice were maintained on a normal chow diet (ND) (PicoLab 5053 Rodent Diet 20; Lab Diets) *ad libitum,* except when the High-fat diet (HFD is indicated.

For high-fat diet (HFD) experiment, mice received a diet containing 42% of calories from fat (TD.88137, Harlan Laboratories, Inc., Indianapolis, IN) for 16 weeks. A single dose of NR (ChromaDex) 500mg/kg body weight was then administered by intraperitoneal (i.p.) injection. Control mice received vehicle (saline) injections. Directly following injection, mice were fasted for 15 hours for assessment of fasted glucose levels and glucose tolerance (GTT). For GTTs, blood was collected

from the tail vein before and 15, 30, 60, and 120 min after i.p. injection of 50% dextrose (1.5g/kg body weight). Blood glucose levels were measured using an AlphaTrak II glucometer (Abbott Laboratories).

For measurements of NR, NMN, NAD^+, and NAM content in blood, mice were fasted overnight before NR (500 mg/kg, i.p.) was administered. Blood was collected from the tail vein at 0-150 min, and 20% trichloroacetic acid (TCA) was added to stop reaction. After extraction by organic solvent, the nucleotide content was determined by HPLC.

Cell Culture

HEK293T and MEFs were cultured in DMEM with 10% FBS, and penicillin/streptomycin (Life Technologies). A549 cells were cultured in RPMI with 10% FBS and penicillin/streptomycin (Life Technologies). Transfections with Flag or Flag-CD38 vector were performed using Lipofectamine 2000 (Life Technologies) and 5μg of total DNA in media without antibiotics. Experiments were performed 48h after transfection.

Electron Microscopy and quantification of mitochondria morphology parameters

Measurements were generated from transmission electron microscopy images with a magnification of ×20,000. Image J software (version 1.42q, National Institutes of Health, Bethesda, MD) was used to calculate all the mitochondrial size and shape parameters by drawing around of each individual mitochondrion analyzed (Picard, et al., 2010). Surface area (mitochondrial size) is reported in squared micrometers; perimeter in micrometers; aspect ratio (AR) is computed as [(major axis)/(minor axis)] and reflects the "length-to-width ratio"; form factor (FF) [(perimeter2)/(4π·surface area)] reflects the complexity and branching aspect of mitochondria; circularity [4π·(surface area/perimeter2)] is one two-dimensional index of sphericity with values of 1 indicating perfect spheroids; and Feret's diameter represents the longest distance (μm) between any two points within a given mitochondrion. Quantification of mitochondrial ultrastructural defects was done by blinded subjects who were asked to classify TEM images based on a score described by Sisková, et al. 2010. Percentages of TEM images with intact mitochondria with normal appearing cristae (Type I); abnormal mitochondria with either swollen, irregular or whorling cristae (Type II); mitochondria with discontinuous outer membrane or deficient cristae (Type III); and mitochondria with both swollen and

deficient cristae or both discontinues outer membrane and swollen cristae (Type IV) have been expressed from a total pool of 8 independent TEM pictures of each group presented to the subjects.

Flow Cytometry

Mouse liver tissue was minced and digested with liberase (Sigma) at 37° C for 15 minutes to make single cell suspensions. Cells were incubated with FC-receptor block (Miltenyi), stained with anti-mouse CD38-PE and Ter119-APC/Cy7 antibodies (Biolegend) for 45 min at 4° C, and subjected to flow cytometry on BD LSRII (BD Biosciences). Zombie NIR dye (Biolegend) was used to discriminate live/dead cells. Data were analyzed with FlowJo software (FlowJo, LLC) using the following gating strategy: 1) erythrocytes ($Ter119^+$) and dead cells were excluded; 2) doublets (FSC-H vs. FSC-A) and debris (SSC-A vs. FSC-A) were excluded; and 3) $CD38^+$ cells were gated (SSC-A vs. CD38-PE).

NAD/NADH UPLC-Mass Spectrometry Method

Instrumentation: The LC-MS system consisted of a Waters Aquity H class ultra-performance liquid chromatography (UPLC) system, containing a quaternary solvent manager and sample manager-FTN coupled to a Xevo TQ-S mass spectrometer (Waters, Milford, MA) equipped with an electrospray ionization (ESI) source. Data was acquired and analyzed by Waters MassLynx v4.1 software.

Chromatographic conditions: The liquid chromatographic separation of NADH and NAD^+ was accomplished using an Agilent Poroshell 120 EC-C18 pre-column (2.1x5mm, 2.7µ, Chrom Tech, Apple Valley, MN) attached to an Agilent Poroshell 120 EC-C18 analytical column (2.1x100mm, 2.7 µm Chrom Tech, Apple Valley, MN) at 40°C, eluted with a gradient mobile phase composed of water with 0.1% formic acid (A) and ACN with 0.1% formic acid (B) with a constant flow rate of 0.5 mL/min and a total run time of 10 min. The elution was initiated at 100% A and held for 2 min, then B was linearly increased from 0-60% B for 4 min, 60% B was held for 1 min, and returned to initial conditions in .2 min, finishing with 2.8 min at 100% A. Auto-sampler temperature was 4°C and sample injection volume was 10 µl. NAD^+ and NADH were eluted at 1.6 and 3.5 minutes respectively. In control experiments we observed that none of the other NAD related metabolites (including NADP, NADPH, ATP, NAADP, NAAD, ADP, cADPR, ADPR, nicotinamide and nicotinic acid co-eluted with either NAD^+ or NADH.

Detection of NAD^+ and NADH were accomplished using the mass spectrometer in positive ESI mode using capillary voltage 3.5 kV, source temp 150°C, desolvation temp 500°C, cone gas flow 150 L/hr, desolvation gas flow 500 L/hr, using multiple reaction monitoring (MRM) scan mode with a dwell time of 0.075 sec. The cone voltages and collision energies were determined by MassLynx-Intellistart, v4.1, software. Values are as follows:

NAD^+ – m/z 664.27>136.09 - cone voltage 54V --- Collision 42 eV

NADH – m/z 666.28>514.17 – cone voltage 56V --- Collision 26 eV

N- Cyclohexyl benzamide – m/z 204.1>122.00 – Cone voltage 80 V – Collision 20 eV

Stock solution preparation: The primary stock solutions were prepared in silanized glass vials as follows: NAD^+ (10 mg/ml in water) and NADH (1 mg/ml in .01 N NaOH, pH 11.9) n-Cyclohexyl benzamide (IS) (100 ug/ml in EtOH) all were stored at -80°C. Working standards were prepared by dilution of the stock solution into the same solutions mentioned above. Daily standard samples were prepared by diluting above stocks 1:20 in water containing 500-ng/ml internal standard.

Mouse tissue samples were prepared as described in the method section. Samples were thawed on ice. Samples were diluted in water containing 500 ng/ml of internal standard. Samples for NAD^+ measurement were diluted 1:1000 and 1:10000, whereas the ones for NADH samples were diluted 1:1000 in slick microfuge tubes. Samples were vortexed and transferred to 2 ml auto-sampler vials for immediate analysis.

NR, NAD+ and NMN Measurements by HPLC

Blood from WT and CD38KO mice after NR or vehicle treatment was collected and extracted by organic solvent and neutralized by NaOH on ice. For measurements, the HPLC was at a flow rate of 0.25 ml/min with 99% buffer A from 0-3 min, a linear gradient to 99% buffer A/1% buffer B (100% methanol) from 3-20 min, 80% buffer A/20% buffer B from 20-21 min, a linear gradient to 30% buffer A/70% buffer B from 21-28 min at 0.35 ml/min, 99% buffer A/1% buffer B from 28-31 min, and a linear gradient to 99% buffer A from 31-37 min at 0.25 mL/min. The protocol was adjusted based on previous studies (Yoshino & Imai, 2013). Concentrations were quantitated based on the peak area compared to a standard curve and normalized to volume of blood collected.

Mitochondria Isolation

After removing the tissue as described in the manuscript, the homogenates were centrifuged at 600 *x g* for 5 min. The supernatant was removed and centrifuged at 7000 *x g* for 10 min. The pellet obtained from spleen was resuspended in the buffer and centrifuged one more time at 7000 *x g* for 10 min. The final spleen pellet was resuspended in respiration buffer (MIR05, described below) for respiration measurements or frozen for other experiments. The pellet obtained from liver was resuspended in isolation buffer containing 15% of percoll (Invitrogen). A percoll gradient was placed in a centrifugation tube starting with isolation buffer containing 40% percoll in the bottom, followed by 22% percoll and 15% percoll at the top containing the pellet. The tube was centrifuged at 25,000 *x g* for 5 min. After the centrifugation, a percoll gradient is formed inside the tube and purified liver mitochondria fraction is placed between the two lower layers. The fraction is removed carefully and resuspended in isolation buffer. Two more centrifugations at 7000 *x g* for 10 min were done to wash out percoll from the sample. The final liver mitochondria pellet was resuspended in MIR05 + BSA fatty acid free 1mg/mL for respiration experiments or frozen for other experiments. Final protein concentration was between 10-15 mg/mL. With this isolation method our mitochondria preparation show an average respiratory control ratio, RCR (state 3^{ADP}/ state 4) of 3.5±0.5.

Mitochondrial Function

Cells - Cells were washed with PBS, trypsinized and resuspended in culture medium without serum. 1-5 x 10^6 cells were added in oxygraph chamber at the same time right before closing the chambers. The basal respiration rate was detected (*routine respiration*) after 15 minutes of oxygen consumption in culture media, oligomycin (2 μg/mL) was added to inhibit ATP synthesis (*leak respiration*), followed by a carefully titration with FCCP (0.2-2.5 mM) until a maximum electron transport capacity was reached (*ETC*). Rotenone (2 μM) + antimycin A (2.5 μM) were added to inhibit mitochondrial respiration and the residual oxygen consumption rate, which was not mitochondria-related, was subtracted from all the other respiration measurements. The respiration coupled to ATP production was calculated by the difference between routine and leak respirations rates (*couple respiration*) (Brand & Nicholls, 2011; Pesta & Gnaiger, 2012). The same protocol was used to perform respirometry in BMDM. Graph shows % of oxygen consumption in *pmol* $O_2/10^6$ *cells.*

Isolated Mitochondria - Mitochondria from liver or spleen (0.1-0.3 mg/mL) were incubated in the oxygraph chamber with an adaptation of MIR05 buffer: 0.5 mM EGTA, 3 mM $MgCl_2$, 20mM Taurine, 10 mM KH_2PO4, 20 mM Hepes, 110 mM D-sucrose, 1 g/L fatty acid–free BSA, 60 mM K-MES. The chamber final volume was 2.1mL. The chambers were closed right before the start of measurements. For isolated mitochondria, after a resting rate was obtained, respiration was induced by adding substrates for complex I or II, 5 mM glutamate/0.5 mM malate (GM) or 10 mM succinate, respectively. Other additions of reagents are indicated in the panel. The graph indicates the flow in pmol of O_2/mg of protein/second, and the respiration rates shown are subtracted from basal levels (mitochondria with no substrates). In Figure S3, a small adaptation of the protocol was performed based on (Kuznetsov et al., 2002) after the succinate step. We measured mitochondrial complex activities through different segments of the electron transport chain. After succinate addition, to activate respiration (CIII) we added 2.5 mM ADP. After this we inhibited complex I with 1 μM rotenone and complex III with 5 mM antimycin A (AA). This was followed by addition of the artificial substrates for complex IV (cytochrome c oxidase, COX), 0.5 mM TMPD, and 2 mM ascorbate. In this case, state 3 respiration (CIII) was determined by rates of (*ADP – AA)*, and CIV by (*TMPD/ascorbate – KCN)* rates. Based on that our measurements were: CI (NADH:ubiquinone oxidoreductase (rotenone sensitive)), CII ($FADH_2$: ubiquinone oxidoreductase), CIII (Ubiquinol-cytochrome *c* oxidoreductase (antimycin-sensitive)), CIV (cytochrome *c*- oxidoreductase (KCN-sensitive)).

Membrane potential was measured by using the fluorescence signal of the cationic dye, safranin-O. Liver mitochondria (0.2 mg protein/mL) were incubated in respiration buffer supplemented with 10 μM safranin O. Fluorescence was detected with an excitation wavelength of 495 nm and an emission wavelength of 586 nm (Spectra Max M5, Molecular Devices). Data are reported as percentage of maximal polarization induced by succinate.

DNA extraction and Mitochondrial Content

Total DNA was extracted from 1-2 x 10^6 cells or 10-20 mg of liver tissue using DNeasy Blood & Tissue Kit (Qiagen). Mitochondrial content was assessed by real-time PCR analysis of the abundance of specific mitochondrial encoded genes relative to nuclear encoded genes using a CFX384 Real-Time System (Bio-Rad). For cells, analysis was performed by the SYBR Green method using primers for NADH dehydrogenase I (ND1) and Actin: (ND1: Forward *5'-TCA AAC TAC GCC CTG*

ATC GG-3' and Reverse *5'-GGA GAG GTT AAA GGA GCC ACT-3';* Actin: Forward *5'-TTC CTT CCT GGG CAT GGA GTC-3'* and Reverse *5'-AGA CAG CAC TGT GTT GGC GTA-3'*) (Amoêdo, et al, 2011). For mouse tissue, analysis was performed using commercially available Taqman probes for cytochrome c oxidase subunit (COX I), NADH dehydrogenase subunit 4 (ND4), and GAPDH, according to the manufacturer's instructions (Applied Biosystems, see table below). Mitochondrial copy number was calculated as ND1 relative to Actin for cells and COX1 or ND4 relative to GAPDH for tissue.

Quantification of mRNA

Omental fat was collected from healthy (BMI 32.8 ± 1.0 kg/m^2) kidney donors aged 30-68 years. The Protocol (10-005236) was approved by the Mayo Clinic Foundation Institutional Review Board for Human Research. Informed consent and consent to publish was obtained from all human subjects. RNA was isolated from human and mouse fat using the Trizol method, and from mouse liver and spleen using the RNeasy Plus Mini kit (Qiagen). cDNA was synthesized using QuantiTect Reverse Transcription kit (Qiagen). Quantitative real-time PCR was performed in triplicates using commercially available TaqMan gene expression probes (Applied Biosystems, see table below), according to the manufacturer's instructions, on a BioRad CFX384 thermal cycler. The relative mRNA abundance of target genes was calculated by the $2^{(-ddCq)}$ method (Livak and Schmittgen, 2001). The expression changes were calculated relative to control. Expression profiles for glucose metabolism and mitochondrial biogenesis pathways were analyzed using Qiagen RT2 Profiler PCR Arrays according to the manufacturer instructions (n=4 per group). RNA quality was assessed using an Agilent2100 Bioanalyzer.

TaqMan Gene Expression Assays

	Gene Symbol	Probe ID
Mouse	*Cd38*	Mm01220906_m1
	Cox1	Mm04225243_g1
	Nadk	Mm00446804_m1
	Nampt	Mm00451938_m1
	Naprt1	Mm01205844_g1
	Nd4	Mm04225294_s1
	Nmnat1	Mm01257929_m1
	Nmnat2	Mm00615393_m1
	Nmnat3	Mm00513791_m1

	Parp1	Mm01321084_m1
	Parp2	Mm00456462_m1
	Sirt1	Mm00490758_m1
	Gapdh	4352932E
Human	*CD38*	Hs01120071_m1
	ND1	Hs00159587_m1
	PARP1	Hs00242302_m1
	NAMPT	Hs00237184_m1
	ACTIN	Hs03023943_g1

SUPPLEMENTAL REFERENCES

Amoêdo ND, Rodrigues MF, Pezzuto P, Galina A, da Costa RM, de Almeida FC, El-Bacha T, Rumjanek FD. Energy metabolism in H460 lung cancer cells: effects of histone deacetylase inhibitors. PLoS ONE. 2011;6(7).

Livak KJ, Schmittgen TD. Analysis of relative gene expression data using real-time quantitative PCR and the 2(-Delta Delta C(T)) Method. Methods. 2001;25:402–408.

Picard M, White K, Turnbull DM. Mitochondrial morphology, topology, and membrane interactions in skeletal muscle: a quantitative three-dimensional electron microscopy study. *Journal of Applied Physiology*. 2013;114(2):161-171.

Sisková Z, Mahad DJ, Pudney C, Campbell G, Cadogan M, Asuni A, O'Connor V, Perry VH. Morphological and functional abnormalities in mitochondria associated with synaptic degeneration in prion disease. Am J Pathol. 2010 Sep;177(3):1411-21**.**